Neuroscience 169 (2010) 932–949

CRITICAL ROLES FOR THE NETRIN RECEPTOR DELETED IN COLORECTAL CANCER IN DOPAMINERGIC NEURONAL PRECURSOR MIGRATION, AXON GUIDANCE, AND AXON ARBORIZATION

B. XU,[a] J. S. GOLDMAN,[a] V. V. RYMAR,[b] C. FORGET,[c] P. S. LO,[a,b] S. J. BULL,[a] E. VEREKER,[a] P. A. BARKER,[a] L. E. TRUDEAU,[c] A. F. SADIKOT[b] AND T. E. KENNEDY[a]*

[a]*Centre for Neuronal Survival, Department of Neurology and Neurosurgery, Montreal Neurological Institute, McGill University, Montreal, QC, Canada H3A 2B4*

[b]*Cone Laboratory, Department of Neurology and Neurosurgery, Montreal Neurological Institute, McGill University, Montreal, QC, Canada H3A 2B4*

[c]*Département de Pharmacologie, Faculté de Médecine, Université de Montréal, Montréal, QC, Canada H3C 3J7*

Abstract—DCC (deleted in colorectal cancer), a receptor for the axon guidance cue netrin-1, is highly expressed by mesencephalic dopaminergic (DA) neurons during development; however, the contribution of DCC to DA development remains largely uncharacterized. DA neurons in ventral mesencephalic nuclei also express UNC5 homologue netrin receptors from late embryogenesis to adulthood, raising the possibility that DA axons could be attracted or repelled by netrins. Examining newborn *dcc* null mice, we report that loss of DCC function results in profound alterations of DA circuitry, including DA progenitor cell migration defects, reduced numbers of DA cells in midbrain nuclei, an anomalous DA ventral commissure, malformed DA innervation of the ventral striatum, and reduced DA innervation of the cerebral cortex. Caspase-3 activation was detected in inappropriately localized DA cells, consistent with apoptosis contributing to reduced cell numbers. *Dcc* heterozygous mice express reduced levels of DCC protein. Although less severely disrupted than *dcc* nulls, newborn and adult *dcc* heterozygotes also have fewer DA neurons in ventral mesenscephalic nuclei. Despite the reduced numbers of DA neurons, newborn *dcc* heterozygotes and nulls exhibit similar DA innervation density as wild-type littermates in the nucleus accumbens core, and adult *dcc* heterozygotes exhibit increased DA innervation in medial prefrontal cortex. A trend towards increased innervation of medial prefrontal cortex was detected in newborn *dcc* heterozygotes, but did not reach statistical significance, suggesting that the increase in adult heterozygotes results from enhanced DA arborization during postnatal development. Consistent with the hypothesis that DCC regulates DA axonal projections, disrupting DCC function in culture inhibits netrin-1 induced DA axon extension and axon branching. Furthermore, disrupting DCC function in isolated DA neurons grown as micro-island cultures reduces the number of autaptic synapses per cell. We conclude that DCC regulates appropriate precursor cell migration, axon guidance, and terminal arborization by DA neurons.

Key words: synaptogenesis, UNC5A, UNC5C, Parkinson's disease, drug addiction, schizophrenia.

Mesencephalic dopaminergic neurons (MDNs) are born, migrate, and extend axons in a series of developmentally overlapping stages. Between E12 and E18 in the mouse, MDNs arise from the isthmic organizer located in the ventricular zone along the aqueduct of Sylvius, and migrate along radial glia toward the ventral pial surface of the mesencephalon (Marchand and Poirier, 1983; Riddle and Pollock, 2003; Shults et al., 1990). At E18, migration is complete. MDNs assume a topography similar to that in adults, and distinct boundaries form outlining substantia nigra (SN) and ventral tegmental area (VTA) (Marchand and Poirier, 1983; Riddle and Pollock, 2003; Shults et al., 1990). Between E16 and birth, dopaminergic (DA) neurons extend axons that course through the medial forebrain bundle (MFB) toward major targets in the striatum and cortex. DA axons then elaborate and refine terminal axon arbors and synaptic connections, resulting in the initial specification of DA projections (Riddle and Pollock, 2003).

Deleted in colorectal cancer (DCC) is a type-1 transmembrane receptor of the Ig superfamily that directs cell migration and axon extension in response to sources of netrin during embryogenesis (Keino-Masu et al., 1996; Fazeli et al., 1997). Netrins are bifunctional guidance cues for migrating cells and axons, depending, in part, on the repertoire of netrin receptors expressed by the responding cell. Chemoattraction requires DCC, while cells expressing DCC and an UNC5 homologue netrin receptor may be attracted or repelled. Intracellular signaling mechanisms, such as the concentration of cAMP and activation of protein kinase A, modulate whether netrin functions as an attractant or repellent (Moore et al., 2007).

DCC is highly expressed by MDNs during embryogenesis and in adulthood (Livesey and Hunt, 1997; Volenec et al., 1998; Osborne et al., 2005), and axon outgrowth assays using explants of embryonic tissue have provided evidence that DCC promotes MDN axon extension in response to an exogenous source of netrin-1 (Lin et al.,

*Corresponding author. Tel: +1-514-398-7136; fax: +1-514-398-1319.
E-mail address: timothy.kennedy@mcgill.ca (T. E. Kennedy).

Abbreviations: AC, anterior commissure; Aca, anterior commissure, anterior limb; AcbC, nucleus accumbens, core; AcbS, nucleus accumbens, shell; BME, basal medium eagle; Cg, cingulate cortex; CPu, caudate putamen; DA, dopaminergic; DAT, dopamine transporter; DCC, deleted in colorectal cancer; DIV, days *in vitro*; Gcc, genu of corpus callosum; MDN, mesencephalic dopaminergic neuron; MFB, medial forebrain bundle; mPFC, medial prefrontal cortex; MRF, midbrain reticular formation; NSP, nigrostriatal pathway; PBS-T, phosphate buffer saline with 0.1% Triton-X-100; SN, A9, substantia nigra; SNC, substantia nigra pars compacta; SNR, substantia nigra pars reticulata; TH, tyrosine hydroxylase; UNC5A, UNC5 homologue A; VTA, A10, ventral tegmental area.

0306-4522/10 $ - see front matter © 2010 IBRO. Published by Elsevier Ltd. All rights reserved.
doi:10.1016/j.neuroscience.2010.05.025

2005). We have reported that adult $dcc^{+/-}$ heterozygous mice exhibit a pronounced change in DA function, including a blunted response to amphetamine, and lack of sensitization to repeated doses (Flores et al., 2005). This study indicated that adult $dcc^{+/-}$ heterozygous mice show a ~20% reduction in the total number of tyrosine hydroxylase (TH)-positive DA neurons in the midbrain, accompanied by significantly increased levels of TH, dopamine, and DA metabolites in medial prefrontal cortex. We concluded that a genetic reduction in *dcc* expression significantly alters DA function in the adult; however, the functional contribution of DCC to the development of MDN circuitry remains uncharacterized.

In the present study, we examined TH-immunoreactivity in the brains of $dcc^{+/+}$, $dcc^{+/-}$ and $dcc^{-/-}$ littermates at embryonic and postnatal ages. We report that genetic reduction ($dcc^{+/-}$) or loss of DCC function ($dcc^{-/-}$) results in aberrant migration of MDN progenitors, a decrease in the number of DA neurons in mesencephalic nuclei, an abnormal DA ventral commissure at the level of the hypothalamus, aberrant development of the ventral striatum, and altered axonal arborization in medial prefrontal cortex. Using primary neuronal culture, we demonstrate that disrupting DCC function in DA neurons inhibits axon extension, axon branching, and reduces synapse formation. These findings provide evidence that DCC is required for appropriate MDN precursor cell migration, influences both long-range axon guidance from DA nuclei to brain target regions, and relatively short-range axonal arborization within target regions.

EXPERIMENTAL PROCEDURES

Animals

All experiments with animals were carried out in accordance with the National Institute of Health Guide for the Care and Use of Laboratory Animals (NIH Publications No. 80-23), and consistent with the Canadian Council on Animal Care guidelines for the use of animals in research. All efforts were made to minimize the number of animals used and their suffering. Adult mice heterozygous for the *dcc* knockout (Fazeli et al., 1997) were obtained from Robert Weinberg (Whitehead Institute for Biomedical Research, Cambridge, MA, USA), and were extensively backcrossed into a CD-1 genetic background. All mice were maintained on an *ad libitum* feeding schedule, and kept on a 12-h light/dark cycle. Embryos and postnatal offspring were genotyped by PCR as described (Serafini et al., 1996; Fazeli et al., 1997).

E14, E18, and E19 embryos were obtained from anesthetized, timed-pregnant mice. The embryos were fixed with 4% paraformaldehyde (PFA) overnight followed by equilibration in 30% sucrose for 2 days. Serial coronal sections, 20 μm, were cut with a cryostat (Leica CM1850, Leica Microsystems Inc., Richmond Hill, ON, Canada) and stored at −80 °C. P0 and 3-month-old littermates were perfused transcardiacally with phosphate buffered saline (PBS) followed by 4% PFA. Brains were removed and post-fixed in 4% PFA overnight, followed by equilibration in 30% sucrose. Serial coronal 40 μm sections were cut with a freezing microtome and stored in antifreeze solution (0.5 M phosphate buffer, 30% ethylene glycerol, 30% glycerol) at −20 °C.

Immunohistochemistry and immunocytochemistry

For bright-field immunohistochemistry, sections were treated with 0.5% H_2O_2 in PBS with 0.1% Triton-X-100 (PBS-T) for 15 min to quench endogenous peroxidase activity. Sections were blocked with 2% horse serum/2% bovine serum albumin in PBS-T at room temperature for 2 h, and incubated with primary antibodies against TH (polyclonal, 1:500, Chemicon Inc, Temecula, CA, USA; monoclonal, 1:1000, Immunostar Inc., Hudson, WI, USA), dopamine transporter (DAT) (1:250, Chemicon, Temecula, CA, USA), netrin-1 (11760) (Manitt et al., 2001), DCC (1:200, A-20 raised in goat, Santa Cruz Biotechnology, Santa Cruz, CA, USA), UNC5C (1:500; rabbit antiserum against mouse UNC5C, also called RCM, provided by Dr. T. Pawson, University of Toronto) (Tong et al., 2001), 9E10 monoclonal against a myc epitope tag (Abcam Inc, Cambridge, MA, USA), and against an HA epitope tag (Abcam Inc.). Antiserum was also raised in rabbits against a peptide sequence unique to UNC5A (GQPDAGLFTVSEAEC) that is conserved in rat, mouse and human UNC5A sequences. Antibodies were affinity purified. The specificity of the UNC5A antibodies and UNC5C antiserum was demonstrated by Western blotting against whole cell homogenates of HEK293 cells transfected to express recombinant rat UNC5A, UNC5B and UNC5C proteins as described (Leonardo et al., 1997). Anti-DCC A-20 was tested on western blots of HEK293 whole cell homogenates expressing rat DCC or rat Neogenin (Keino-Masu et al., 1996).

For immunohistochemical analysis of cleaved caspase-3 in TH positive cells, E19 embryos were perfused transcardially with 4% PFA. Coronal 50 μm sections were cut with a freezing microtome and stored in antifreeze solution as described above. Sections were immunostained with a rabbit monoclonal antibody against cleaved caspase-3 (1:600, 5A1E, Cell Signaling Technology, MA, USA), a mouse monoclonal antibody against TH (1:1000, Immunostar Inc, WI, USA), and histochemically stained with Hoechst dye to label nuclei.

For bright field immunohistochemistry reactivity was visualized using a biotinylated secondary anti-rabbit antibody (1:1000, Vector Laboratory Inc., Burlingame, CA, USA) and the ABC DAB kit (Vector Laboratory). For immunoflorescence, sections were blocked and incubated with primary antibody as described above and visualized with Alexa fluor® conjugated secondary antibodies (1:1000, Invitrogen Inc., Carlsbad, CA, USA).

Quantification of TH immunoreactivity

Image analysis and quantification of TH immunoreactivity was conducted by an individual blind to the experimental conditions.

Stereological analysis of midbrain DA neurons. Unbiased estimates of the number of midbrain DA neurons were obtained using the optical dissector method as described (van den Munckhof et al., 2003). The rostrocaudal extent of the midbrain was examined in TH-stained 40 μm thick coronal serial sections of newborn $dcc^{-/-}$ homozygous null, $dcc^{+/-}$ heterozygous, and wild-type littermate mice. TH cell counts of every fourth section were conducted at 100× magnification using a 60×60 μm^2 counting frame. Sections counted correspond to levels −2.80, −3.16, −3.52, −3.80, −4.16, −4.48 (160 μm interval), with respect to Bregma (Franklin and Paxinos, 2008). A 10 μm dissector was placed 2 μm below the surface of the section at counting sites located at 150 μm intervals after a random start. Mesencephalic DA nuclei, including VTA, substantia nigra pars compacta (SNC), substantia nigra pars reticulata (SNR), and retrorubral field were examined. Estimates of the total number of TH-positive neurons in mesencephalon and within each nucleus were obtained and analyzed using an ANOVA and Tukey's HSD post-hoc test.

Migration errors of midbrain DA neurons. To estimate the total number of mis-migrated cells the optical dissector was applied to count TH-positive neurons located in the midbrain reticular

formation (MRF). TH immunostained 40 μm thick coronal sections from newborn pups were counted at levels corresponding to −2.46, −2.80, −3.16, −3.52, −3.80, −4.16, −4.48, −4.84 (160 μm interval), with respect to Bregma (Franklin and Paxinos, 2008). The area counted was restricted to a region defined by boundaries drawn 50 μm from the edge of the SN (A9), the VTA (A10), and retrorubral field (A8) (Dalhstrom and Fuxe, 1964; Hynes and Rosenthal, 1999) extending to a horizontal line drawn ventral to the DA neurons of the periaqueductal gray and extending perpendicular to the midline, to the pial surface. The grid of sampled sites was reduced from a 150 to 80 μm interval, to facilitate unbiased detection of the sparse and inhomogeneous distribution of mis-migrated TH-immunoreactive neurons. Statistical significance was assessed using an ANOVA and Tukey's HSD post-hoc test.

Nucleus accumbens core (AcbC) and dorsal striatum. TH immunoreactivity in the nucleus accumbens core was measured by randomly placing four open 80 μm diameter circles around the anterior limb of the anterior commissure (aca). The aca is absent in $dcc^{-/-}$ mice and in these animals circles were placed in comparable positions to wild types within AcbC. Serial sections containing the aca at 60 μm (E18), 160 μm (P0) or 240 μm (adult) apart were measured. The average optical density was obtained for each animal and compared using ANOVA and Tukey's HSD post-hoc test. At E14, the nucleus accumbens has not yet formed, and therefore this age was not included in this analysis. The intensity of TH staining in dorsal striatum was assessed in coronal brain sections of wild type, *dcc* heterozygote, and *dcc* null newborn littermates at three rostrocaudal levels, corresponding to 1.7, 0.74 and 0 mm relative to Bregma. The dorsal striatum was outlined as described (Shatzmiller et al., 2008), using the polygon selection tool in Image J (U. S. National Institutes of Health, Bethesda, MD, USA) and the average optical density of the region calculated.

Medial prefrontal cortex. For all adult littermates, sections from three comparable levels containing cingulate cortex area 1 (Cg1), 2 (Cg2), and 3 (Cg3) were examined. These levels were defined based on the following criteria: (1) the rostal level was the most rostal section in which TH-positive caudate putamen (CPu) was clearly visible, bregma +1.70 mm; (2) the middle level was defined as the most rostal section in which the genu of corpus callosum (gcc) appears, bregma +1.62 mm; and (3) the caudal level was the section in which the anterior commissure (AC) crosses the midline, bregma 0.0 mm.

For P0 fetuses, only the first two levels were examined due to the absence of TH immunoreactivity at the most caudal level. At ages E14 and E18, TH-positive fibers within the prefrontal cortex were either completely absent or extremely sparse, and were therefore not included in the analysis.

After imaging TH-immunoreactivity, coverslips were removed in xylene, and sections post-stained with Cresyl Violet to identify cortical layers. Layer I, II/III, and V/VI on the digital images of TH-immunohistochemistry were outlined based on the Cresyl Violet staining obtained. TH-immunohistochemistry within each defined cortical layer was then measured using North Eclipse software (Empix Imaging Inc., Missisauga, ON, Canada). Surface area occupied by TH-positive fibers was quantified, and subjected to an ANOVA with post hoc Tukey test.

TH immunoreactivity in the superficial layers of the prefrontal cortex in adult $dcc^{+/-}$ and $dcc^{-/-}$ littermates was also detected in coronal sections using immunofluorescence and imaged with a Zeiss LSM 510 confocal microscope. To assess the density of TH positive axonal puncta within the superficial layers of cingulate cortex, 230×230 μm^2 frames encompassing layer I and a portion of layer II were placed in cingulate cortex, within the rostral section described above. The number of TH-IR puncta was counted, and compared between genotypes using an ANOVA and post hoc Tukey test.

Embryonic mesencephalic cell culture

Ventral mesencephalic cell cultures were prepared from E13.5 CD1 mouse embryos as previously described (Berger et al., 1982; Shimoda et al., 1992) with several modifications. Briefly, ventral mesencephalon was dissected in ice cold Hank's Balanced Salt Solution, diced, and incubated for 20 min at 37 °C in Hepes-buffered Standard Minimum Essential Medium containing 0.25% Trypsin and 0.001% DNase I. The tissue was then washed once in ice-cold Neurobasal supplemented with 10% heat-inactivated fetal bovine serum (hiFBS) and gently triturated with a flamed Pasteur pipette to yield a suspension of dispersed single cells. Cells were plated at 100,000 cells/cm^2, a medium density that facilitates survival of DA neurons (Shimoda et al., 1992). Cultures were maintained for up to 8 days *in vitro* (DIV) in neurobasal medium containing 5% hiFBS, 1% B27, 0.5% N2, 2 mM glutamine, 1 U/mL penicillin, and 1 μg/mL streptomycinin at 37 °C in a humidified 5% CO_2 incubator. Half the total volume was changed every 4 days with fresh media, but without penicillin and streptomycin.

Axon branching analysis was performed according to a previously established protocol (Aoyagi et al., 1994), with all axon processes greater than 20 μm in length being counted as branches. The total number of branch points per axon was scored and normalized as a function of branches per 100 μm axon length. Axon length and axon branching was measured for between 43 to 59 neurons per experimental condition, and subjected to one-way ANOVA followed by post hoc Tukey test. To investigate whether netrin-1 and its receptors were expressed by mesencephalic DA neurons *in vitro*, 8 DIV mesencephalic cultures were fixed with 4% PFA in PBS, and stained with antibodies against netrin-1, DCC, UNC5C, or UNC5A, together with antibodies against TH, as described above.

Postnatal DA neuron microculture

Quantification of axon terminal number was performed on isolated DA neurons in microcultures as described (Fasano et al., 2008). Neurons were grown on small droplets of substrate that limit synaptic connectivity to the cells within the droplets. Coverslips were coated with poly-L-ornithine and then agarose, a substrate that prevents cell adhesion. Collagen was applied on top of the agarose using a micro-sprayer, thus establishing islands of substrate suitable for cell growth. Neonatal (P0 to P2) Sprague–Dawley rats were cryoanaesthetized. Brains were rapidly removed and transferred into ice-cold dissociation solution. A block of tissue containing DA neuron cell bodies was microdissected from a 1-mm-thick slice cut at the level of the midbrain flexure. Blocks were digested in papaïn for 30 min at 37 °C before being gently triturated. The dissociated cells were collected by centrifugation, counted, and plated at a concentration of 100,000 cells/mL onto the coverslip patterned with micro-islands onto which astrocytes had been previously plated. In order to provide an extracellular milieu as rich as possible in natural growth factors, a flask plated with astrocytes was filled with BME (Basal Medium Eagle) for 2 weeks to produce conditioned medium (BME+). Neuronal cultures were maintained in a solution composed of (1:3) BME+ and Neurobasal A supplemented with penicillin/streptomycin, GlutaMAX-1, 10% fetal bovine serum (GIBCO, USA) and B27 serum extender (Invitrogen). FUdR was added to the medium 24 h after neurons were plated to prevent cell division of newly plated cells. Cell culture media was changed at 2 DIV and 4 DIV, and cells were fixed for analysis at 7 DIV. Cell cultures were incubated at 37 °C in a 5% CO_2 atmosphere.

For immunostaining, cells were fixed with 100% methanol for 5 min at 4 °C, permeabilized with 0.1% triton X-100 for 10 min and blocked for 5 min in a solution containing BSA (0.5%). Cells were then labelled with a rabbit monoclonal antibody against TH (1:

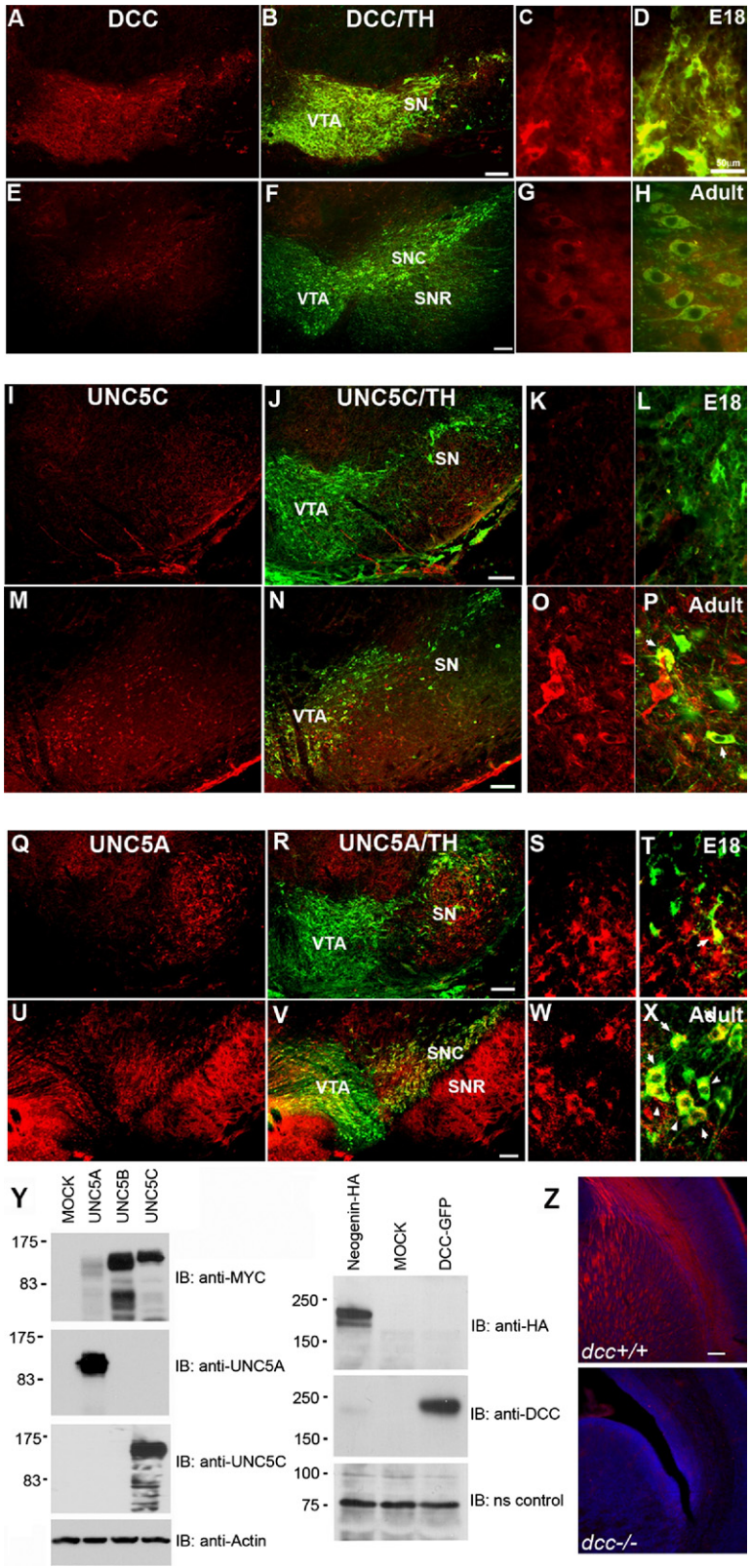

Fig. 1. Expression of netrin receptors, DCC, UNC5A, and UNC5C in MDNs at E18 and in adulthood. (A–H) Expression of DCC in E18 and mature mesencephalic DA nuclei. Sections are double-labeled with antibodies against DCC (red) and TH (green). (B, F, D, H) Midbrain sections stained for DCC and TH. (D, H) SN neurons at high magnification. (I–X) UNC5 homologue (red) and TH-immunoreactivity (green) in mesencephalic DA neurons. Sections are stained either with an UNC5C antibody (I–P) or an UNC5A antibody (Q–X). White arrowheads (P, T, X) identify TH and UNC5 homologue

1000; Pel-Freez Biological, USA) and a mouse monoclonal anti-SV2 antibody (1:500; Developmental Studies Hybridoma Bank, IA, USA). Primary antibodies were detected using Alexa-488 or Alexa-647 coupled secondary antibodies (1:200, Molecular Probes Inc., Eugene, OR, USA). Images were acquired using a point-scanning confocal microscope from Prairie Technologies LLC (Middleton, WI, USA) and analysed using Metamorph software v4.5 from Universal Imaging Corp (Downingtown, PA, USA).

RESULTS

Netrin receptor expression in midbrain DA neurons during development

To assess the contribution of DCC to the development of DA circuitry we first carried out an immunohistochemical analysis of DCC expression by ventral midbrain DA neurons. To characterize the specificity of the A-20 DCC antibody, we first demonstrated selective binding to recombinant DCC protein, but not the DCC paralogue Neogenin, on western blots of whole cell homogenates (Fig. 1Y). Further supporting the specificity of the antibody, DCC immunoreactive neuronal cell bodies and axons were readily detected on a section of E19 wild type mouse brain, but were absent from a corresponding section of a $dcc^{-/-}$ null littermate (Fig. 1Z).

In brain sections of E18 wild type mice, DCC immunoreactivity was detected in most TH-positive neurons located in SN and VTA (Fig. 1A–D). In the adult mouse brain, DCC expression was readily detected in DA neurons (Fig. 1E–H), but at levels lower than those found during development, consistent with previous findings in rat and mouse (Osborne et al., 2005; Livesey and Hunt, 1997).

Cells that express DCC and an UNC5 homologue may respond to netrin-1 as an attractant or a repellent (Moore et al., 2007; Hong et al., 1999). To assess UNC5 homologue expression by DA neurons during development, we obtained a polyclonal antiserum against mouse UNC5C (Tong et al., 2001; Manitt et al., 2004), and generated a polyclonal antiserum against a peptide sequence specific for UNC5A. Western blot analyses of recombinant UNC5 proteins in whole cell lysates using these antibodies demonstrated selective binding to UNC5C and UNC5A, respectively (Fig. 1Y).

In ventral mesencephalon at E18, UNC5A and UNC5C immunoreactivity was detected in SN and VTA, however only a subset of neurons were positive for both TH and either UNC5A or UNC5C (Fig. 1I–L, Q–T). In contrast, in adulthood, most midbrain TH positive DA neurons expressed readily detectable UNC5 homologue immunoreactivity, with UNC5A being more widely expressed than UNC5C (Fig. 1M–P, U–X). These findings are consistent with positive *in situ* hybridization for UNC5A and UNC5C in DA nuclei of mature mouse brain (Allen Brain Atlas Internet. Seattle (WA): Allen Institute for Brain Science. © 2004–2007. Available from:http://www.brain-map.org). While these findings do not rule out expression of UNC5B and UNC5D by DA neurons, they support the conclusion that UNC5 homologues are expressed by DA neurons during development and in adulthood.

Reduced numbers of TH-positive neurons in $dcc^{-/-}$ newborn mice

TH-positive DA progenitors migrate rostrally and radially from the aqueduct of Sylvius to the developing SN and VTA between E12–E18 (Marchand and Poirier, 1983; Shults et al., 1990). Immunohistochemical double-labeling indicated that migrating TH-positive neurons express DCC in E14 wild type embryos (Fig. 2K–N). We therefore examined TH-positive cells in $dcc^{+/+}$ wild type, $dcc^{+/-}$ heterozygote, and $dcc^{-/-}$ null E14, E18, and P0 littermates to determine if DCC function contributes to appropriate cell migration (Fig. 2A–I).

To determine if the loss of DCC function might influence the number of DA neurons present, an estimate of the total number of TH-positive cells localized to midbrain DA nuclei was obtained using stereological counting. The total number of TH-positive cells within ventral midbrain DA nuclei, including the number of cells within the SNC, SNR, VTA and retrorubral field, was significantly decreased in both newborn $dcc^{+/-}$ heterozygotes and $dcc^{-/-}$ null pups when compared with wild-type littermates (Fig. 2J). The coronal sections counted correspond approximately to levels −2.80, −3.16, −3.52, −3.80, −4.16, −4.48, with respect to Bregma (Franklin and Paxinos, 2008).

DA precursor cells normally complete their migration by E18 in mice and at this point a distinct boundary outlining the SN and VTA has formed (Marchand and Poirier, 1983; Shults et al., 1990). In wild type and $dcc^{+/-}$ heterozygous mice, few TH-positive cells are located outside

double-labeled neurons. Scale bars: 300 μm in (B, F, J. N, R, V); 50 μm in (D). (Y) HEK293 cells were transfected with expression vectors encoding full length rat UNC5A, UNC5B, and UNC5C, each of which encodes a C-terminal myc epitope tag. Immunoblots of whole cell homogenates were probed with the 9E10 monoclonal antibody which binds the myc epitopte tag, revealing expression of full length recombinant UNC5 homologue proteins ranging in size from approximately 130 to approximately 150 kDa. Although relatively low levels of UNC5A were expressed by the cells, polyclonal antibodies raised against an UNC5A specific amino acid sequence and affinity purified from the rabbit antiserum detect a robust band selectively in the UNC5A transfected whole cell homogenate. The antiserum raised against mouse UNC5C detects a strong signal selectively in the UNC5C transfected cells. The blots shown were intentionally over-exposed to demonstrate the absence of off-target cross reactivity. Actin immunoreactivity demonstrates approximately equal amounts of protein loaded per lane. HEK293 cells were transfected with expression vectors encoding full length rat Neogenin encoding a c-terminal HA tag, or encoding rat DCC fused at its c-terminus to GFP (Shekarabi and Kennedy, 2002). Expression of full length Neogenin was detected using an antibody against the HA epitope tag. Probing the same whole cell homogenates with the A-20 goat polyclonal anti-DCC readily detects DCC, but not Neogenin. A non-specific ~75 kDa band detected in the whole cell homogenates by the HA antibody demonstrates approximately equal amounts of protein loaded per lane. (Z) Wild type E19 mouse brain (top) stained with A-20 goat polyclonal anti-DCC (red), compared to a brain section from a $dcc^{-/-}$ null littermate, illustrating the absence of DCC immunoreactivity in the knockout (nuclei stained blue with Hoechst dye, coronal sections containing dorsal striatum, neocortex and corpus callosum, 10× objective lens, scale bar corresponds to 100 μm).

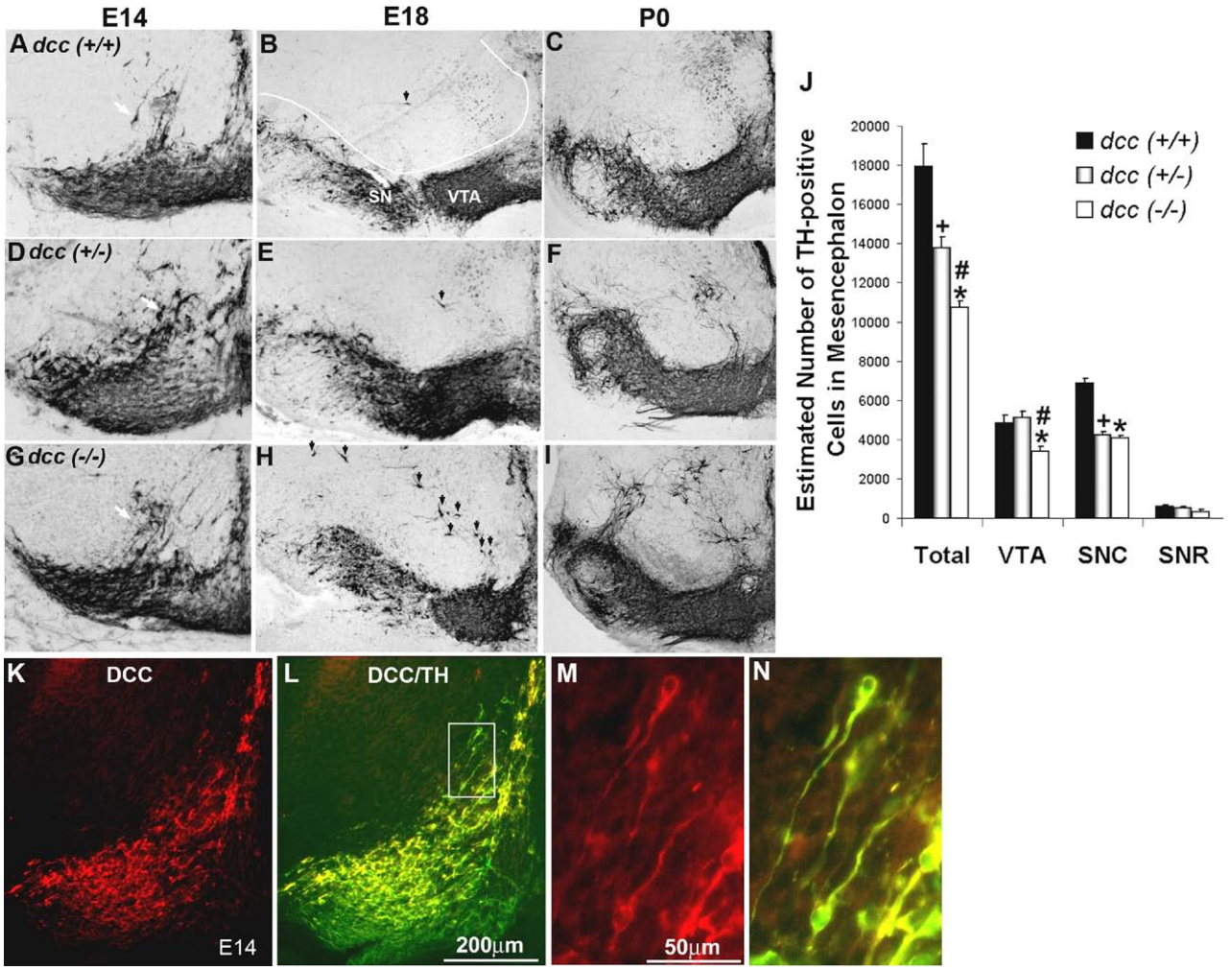

Fig. 2. Reduced number of TH-positive neurons in midbrain DA nuclei in newborn $dcc^{+/-}$, and $dcc^{-/-}$ mice. (A–I) Representative midbrain sections of wild type $dcc^{+/+}$ (A–C), $dcc^{+/-}$ heterozygotes (D–F), and $dcc^{-/-}$ null mice (G–I). At E14, migrating tyrosine hydroxylase (TH)-positive cells (white arrows in (A), (D), and (G)) were observed between the aqueduct of Sylvius and VTA/SN in all genotypes. By E18, when migration of midbrain DA neurons is normally complete, TH-positive cells were rarely found outside the VTA or SN in wild type mice (B). In contrast, numerous TH-positive neurons were located between the aqueduct of Sylvius and SN/VTA in $dcc^{-/-}$ mice (H). Inappropriately positioned TH-positive neurons were still present at P0 (I). Black arrowheads (B, E, H) indicate inappropriately positioned TH-positive neurons located more than 50 μm outside of the VTA/SN boundary (white line in B). (J) Stereological estimates of the total number of TH-positive cells in DA nuclei in the midbrain of newborn pups reveals an approximate 40% reduction in $dcc^{-/-}$ and 20% reduction in $dcc^{+/-}$ mice as compared to wild-type littermates (ANOVA, post-hoc Tukey test, * $P<0.005$ between $dcc^{+/+}$ and $dcc^{-/-}$; $^{+}$ $P<0.05$ between $dcc^{+/+}$ and $dcc^{+/-}$; $^{\#}$ $P<0.05$ between $dcc^{+/-}$ and $dcc^{-/-}$, three P0 pups of each genotype). (K–N) Immunofluorescent images derived from E14 $dcc^{+/+}$ mice. DCC immunoreactivity is shown in red (K, M) and TH in green (merges in L and N). At E14, the majority of TH-positive neurons also express DCC.

this boundary (Fig. 2B, C, E, F). In contrast, in $dcc^{-/-}$ null mice misplaced TH-positive cells were present within the midbrain reticular formation between the aqueduct of Sylvius and SN/VTA (Fig. 2H, I). We therefore assessed the number of misplaced cells present, to determine if they might account for the reduced cell numbers found in midbrain DA nuclei.

Aberrant midbrain DA neuronal migration in DCC deficient mice

To assess the accuracy of cell migration, the optical fractionator was used to obtain stereological estimates of the total number of TH-immunoreactive neurons aberrantly located within the midbrain but outside of the ventral midbrain DA nuclei. TH positive cells were counted within a region bounded by lines drawn 50 μm from the dorsal limits of the substantia nigra (SN, A9), ventral tegmental area (VTA, A10), and retrorubral field (A8) (Dalhstrom and Fuxe, 1964; Hynes and Rosenthal, 1999), then up to a horizontal boundary just below the DA neurons of the periaqueductal gray and extending perpendicularly from the midline to the lateral pial surface (see Fig. 3A). This analysis detected an approximately threefold increase in the number of migration errors in $dcc^{-/-}$ knockout newborn pups compared to either wild type or $dcc^{+/-}$ heterozygote littermates. Wild type and heterozygote pups were not significantly different using this measure (Fig. 3B). The estimate of the number of misplaced cells (Fig. 3B) was

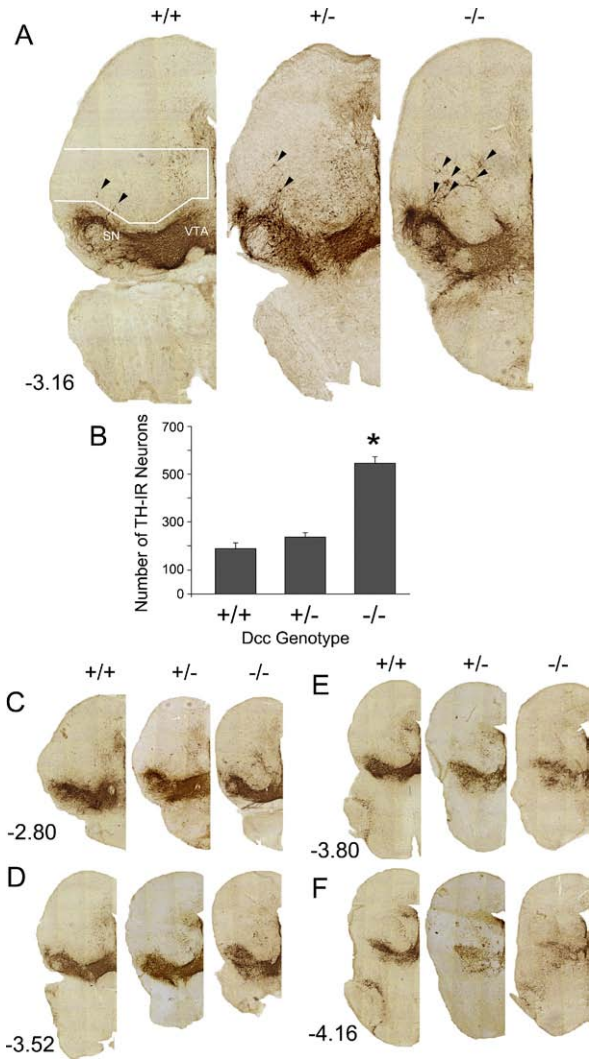

Fig. 3. Disruption of DA neuronal migration in DCC null newborn mice. (A) The number of TH-immunoreactive cells aberrantly located within the midbrain but outside of ventral midbrain DA nuclei in newborn mice was assessed using the optical fractionator. Three newborn (P0) pups of each *dcc* genotype, wild type $dcc^{+/+}$, heterozygote $dcc^{+/-}$ and null $dcc^{-/-}$, for a total of nine littermates, were examined. Eight coronal sections were chosen that correspond to levels −2.46, −2.80, −3.16, −3.52, −3.80, −4.16, −4.48, −4.84, with respect to Bregma. Dorsal is toward the top and the midline is at the right side in all images. Panel (A) illustrates three representative brain sections (−3.16 with respect to Bregma), one for each genotype as indicated, stained for TH immunoreactivity. Displaced TH positive cells were counted within a region bounded as indicated by the white line depicted in the section from wild type brain in panel (A). The limits were drawn 50 μm from edge of the SN (A9), VTA (A10), and retrorubral field (A8), to a horizontal boundary just below the DA neurons of the periaqueductal gray that extends perpendicularly from the midline to the lateral pial surface. Displaced TH positive cell bodies or clusters of cell bodies representative of those counted are indicated with black arrowheads. (B) An approximately threefold increase in the number of displaced cells was detected in $dcc^{-/-}$ knockout newborn pups compared to either wild type or heterozygote $dcc^{+/-}$ littermates. The number of displaced cells found in wild type and heterozygote pups was not significantly different. Note that the increased TH staining present dorsal of the SN and VTA in the heterozygote section illustrated in panel (A) corresponds TH positive fiber tracts and not an increase in the number of cell bodies. Statistical significance was assessed using an ANOVA and Tukey's HSD test. * corresponds to $P<0.01$, between wild type and knockout. Panels (C–F) illustrate three representative brain sections, one for each genotype, stained for TH immunoreactivity, at levels −2.80, −3.52, −3.80, and −4.16, with respect to Bregma.

substantially less than the estimated numbers of cells missing from midbrain DA nuclei in $dcc^{+/-}$ heterozygotes and $dcc^{-/-}$ knockouts, indicating that the errors in cell migration detected do not fully account for the reduced cell numbers.

To determine if apoptosis might contribute to eliminating cells inappropriately positioned dorsal to SN and VTA, brain sections from E19 wild type, $dcc^{+/-}$ heterozygote, and $dcc^{-/-}$ knockout littermates were immunostained for TH and activated caspase-3. Consistent with the findings illustrated in Figs. 2 and 3, a scattered population of TH positive cells was inappropriately located dorsal to SN in $dcc^{-/-}$ knockout mice (Fig. 4A, D–F). Immunoreactivity for activated caspase-3, indicating ongoing apoptosis (Riedl and Salvesen, 2007), was detected in a subpopulation of these cells. A population of cells positive for activated caspase-3, in which TH immunoreactivity was not detected, was also present. While caspase-3 positive cells were also detected in wild type and $dcc^{+/-}$ heterozygous mice, fewer cells were apparent than in $dcc^{-/-}$ knockouts, and wild type and heterozygous mice did not exhibit the relatively large number of dorsally displaced TH positive cells present in the knockouts. These findings provide evidence that apoptosis of misplaced cells contributes to the reduced number of MDNs in mice lacking DCC function.

Aberrant axon targeting and innervation in DCC deficient mice

In all three genotypes—wild type, heterozygote, and null—the invasion of DA fibers into target structures initially followed a temporal and spatial pattern appropriate for that previously reported in mice (Riddle and Pollock, 2003; Voorn et al., 1988). In E18 brain sections, large bundles of TH-positive fibers were detected in the dorsal and ventral striatum, and a smaller proportion of TH-positive fibers projects toward the cortex. Scattered TH-positive fibers were detected in the prefrontal cortex of all three genotypes at E18 (data not shown).

In newborn $dcc^{-/-}$ knockout mice, analysis of the gross distribution of DA nuclei and axonal projections revealed a similar distribution to that in wild type littermate newborns (Fig. 5). DA cell bodies located in the olfactory bulb (A16), diencephalon (A11–15), and ventral mesencephalon (A8–A10) (Dalhstrom and Fuxe, 1964; Hynes and Rosenthal, 1999) exhibited a normal distribution in $dcc^{-/-}$ null mice. The architecture of mesolimbic and mesostriatal DA projections in $dcc^{-/-}$ mice was similar to that of $dcc^{+/+}$ mice with the following exceptions: in the absence of DCC (1) an aberrant ventral commissure descended from the MFB, and crossed the midline at the level of the hypothalamus (Fig. 5E, F);

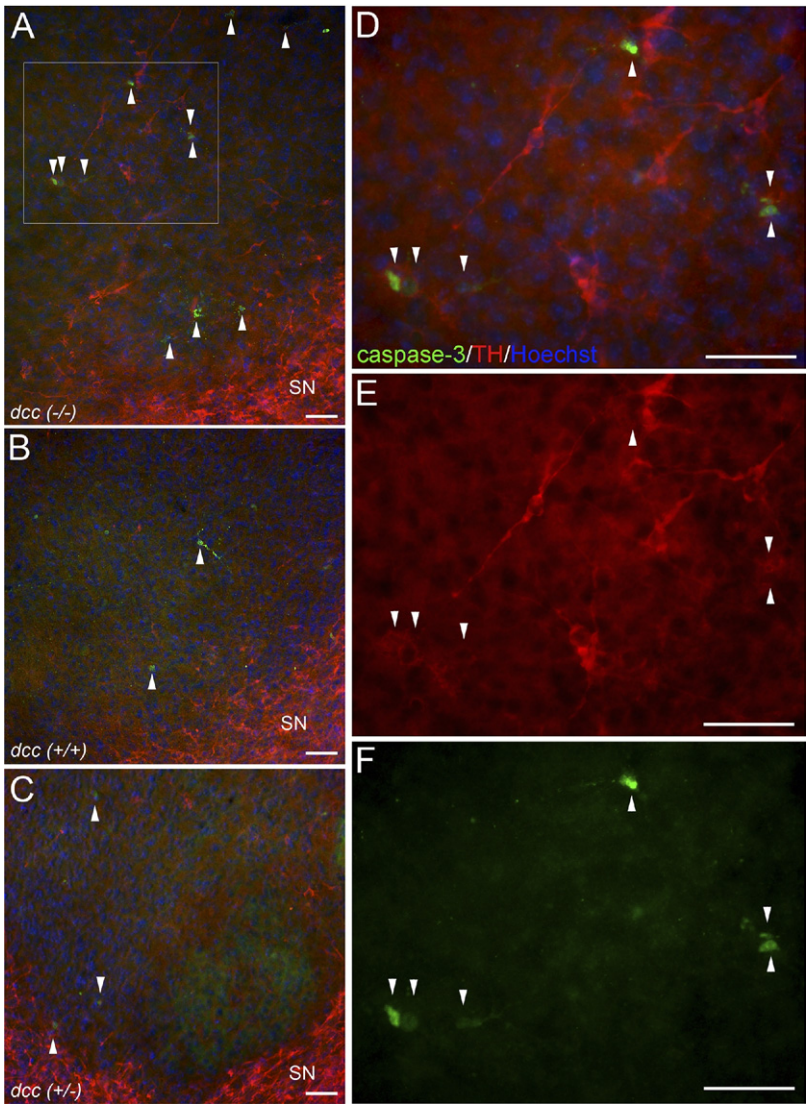

Fig. 4. Detection of activated caspase-3 in mis-migrated cells in E19 wild type, $dcc^{-/-}$, and $dcc^{+/-}$ mice. Florescent immunohistochemical detection of TH (red), activated (cleaved) caspase-3 (green), and Hoechst stain for nuclei (blue), in coronal sections of E19 (A) $dcc^{-/-}$ knockout, (B) wild type $dcc^{+/+}$ and (C) $dcc^{+/-}$ heterozygous mice. In (A–C), the dorsal edge of the substantia nigra (SN) is visible to the lower left. A large number of TH positive cells are detected inappropriately dorsal to the SN in $dcc^{-/-}$ knockout sections, consistent with the quantification presented in Fig. 3. Upward pointing arrowheads identify cells in which both TH and cleaved caspase-3 immunoreactivity was detected. Downward pointing arrowheads identify cleaved caspase-3 positive cells that were not detectably TH positive. Panels (D–F) are a higher magnification image (40× objective lens) of the region boxed in panel A (20× objective lens). (Panels D–F) illustrate immunoreactivity for TH and cleaved caspase-3, and Hoechst staining, respectively. In all panels, (A–F), dorsal is up, and the midline is to the right. The scale bars correspond to 100 μm in all panels.

(2) the TH positive innervation of the ventral striatum, including olfactory tubercle and nucleus accumbens shell (AcbS), was shifted dorsally (Fig. 5C, D), possibly due to reorganization of the mesolimbic projection or the target area itself.

DA axons coursing through the MFB normally project only to ipsilateral structures and never cross the midline (Riddle and Pollock, 2003). Consistent with this, TH-positive fibers were never observed to cross the midline in $dcc^{+/-}$ heterozygotes (data not shown) or wild-type mice at either E18 or P0 (Fig. 5). In contrast, in brain sections of E18 and P0 $dcc^{-/-}$ null mice, a striking abnormal projection of TH positive axons was detected crossing the ventral midline at the level of the hypothalamus (Figs. 5E, F and 6). This aberrant projection descended from the MFB with axons coalescing into thick fasciculated bundles as they crossed the midline (Fig. 6), and was detected in all $dcc^{-/-}$ null mice examined. Positive dopamine transporter (DAT) immunostaining confirmed that the axons were indeed dopaminergic (Fig. 6E, F).

We then examined the density of TH positive projections in different brain regions. The density of TH labeling within the core of the nucleus accumbens, as measured by the average gray value in the region surrounding the anterior limb of the anterior commissure, did not differ between genotypes at E18 and in adults (Fig. 7). However, at

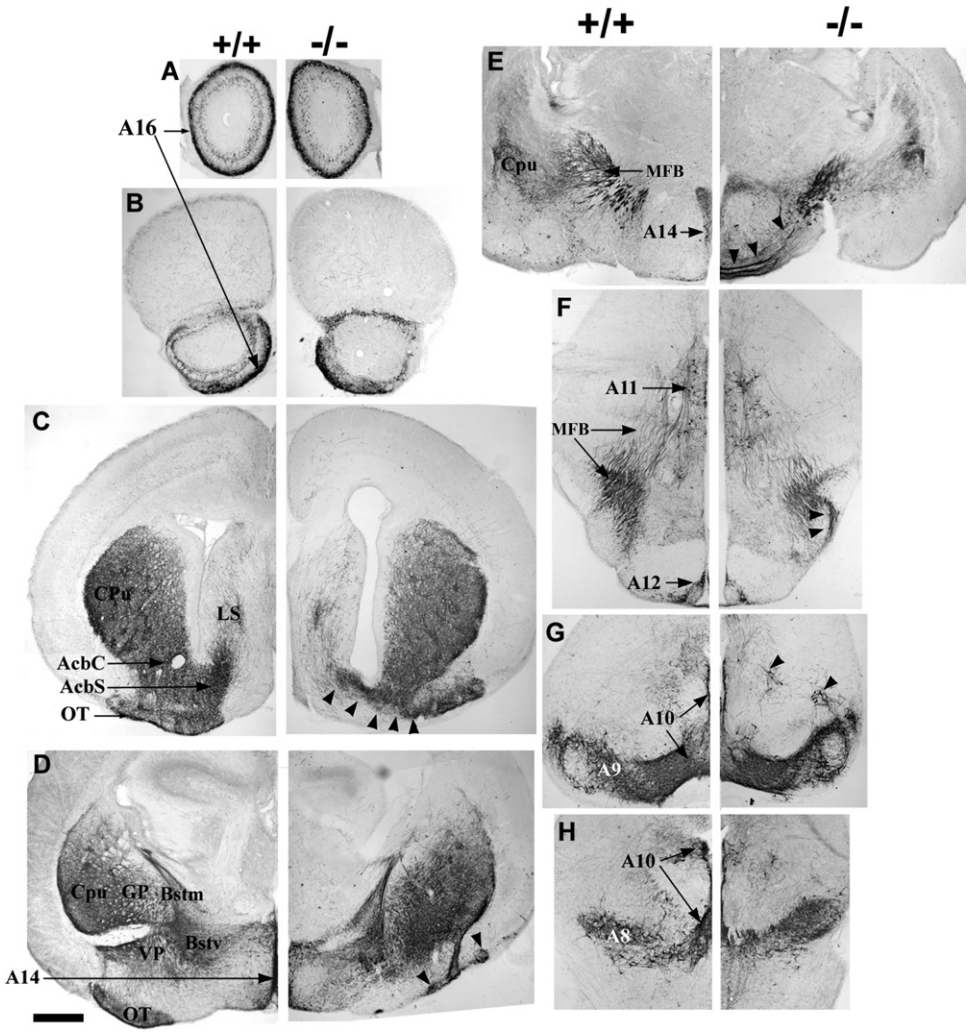

Fig. 5. Overview of DA circuitry in newborn (P0) $dcc^{-/-}$ and $dcc^{+/+}$ mice. The left portion of each panel corresponds to a $dcc^{+/+}$ mouse, and the right portion to a $dcc^{-/-}$ mouse. Representative distribution of TH immunostaining detected in sections of telencephalon (A–C), diencephalon (D–F), and mesencephalon (G, H) from each genotype are shown. (C, D) The ventral striatum, including nucleus accumbens shell (AcbS) and olfactory tubercle (OT), does not develop normally in $dcc^{-/-}$ mice (arrowheads in C and D). (E, F) In $dcc^{-/-}$ mice, an abnormal commissure descends from the MFB, forms thick fasciculated bundles, and crosses the midline in the hypothalamus (arrowheads in E and F). (C–G) Arrowheads indicate misplaced TH-positive neuronal cell bodies and projections in ventral mesencephalon. A16, A16 DA cell bodies, olfactory bulb; AcbC, nucleus accumbens core; GP, globus pallidus; VP, ventral pallidum; Bstm, bed nucleus of the stria terminalis (medial); Bstv, bed nucleus of the stria terminalis (ventral); A14, A14 DA cell bodies; A12, A12 DA cell bodies; A11, A11 DA cell bodies; A10, VTA, A10 DA cell bodies; A9, SN, A9 DA cell bodies; A8, retrorubral field, A8 DA cell bodies. Scale bar in (D) corresponds to 0.5 mm.

P0, a small but significant increase in TH immunoreactivity was detected in $dcc^{+/-}$ heterozygotes compared with wild type littermates (Fig. 7I).

In an earlier study (Flores et al., 2005), we found no significant difference between levels of TH, DA or the DA metabolites DOPAC and HVA in the dorsal striatum of adult wild type and $dcc^{+/-}$ heterozgote aged matched littermates. In the current study, the boundaries of the dorsal striatum were delineated as described (Shatzmiller et al., 2008), and the average density of TH labeling quantified as described above for the nucleus accumbens. No significant change in the density of TH innervations of the neostriatum was detected in $dcc^{+/-}$ heterozygous or $dcc^{-/-}$ null mice at birth (wt: 155±4.0, $dcc^{+/-}$: 149±3.5, $dcc^{-/-}$: 144±2.8, mean optical density±SEM, n=3 pups of each genotype).

We have previously reported ~50% increase of TH protein, in addition to increases in DA and the DA metabolites DOPAC and HVA, in the medial prefrontal cortex in adult $dcc^{+/-}$ heterozygotes compared to wild-type littermates (Flores et al., 2005). Consistent with these findings, using immunohistochemical analysis we detected an increase in the density of TH-positive fiber arborization in sections of prefrontal cortex (Fig. 8). Although the overall size of the medial prefrontal cortex did not differ significantly between genotypes (Fig. 8F, H), the relative surface area occupied by TH-immunoreactive fibers increased by ~50% to 70% in Layer I and

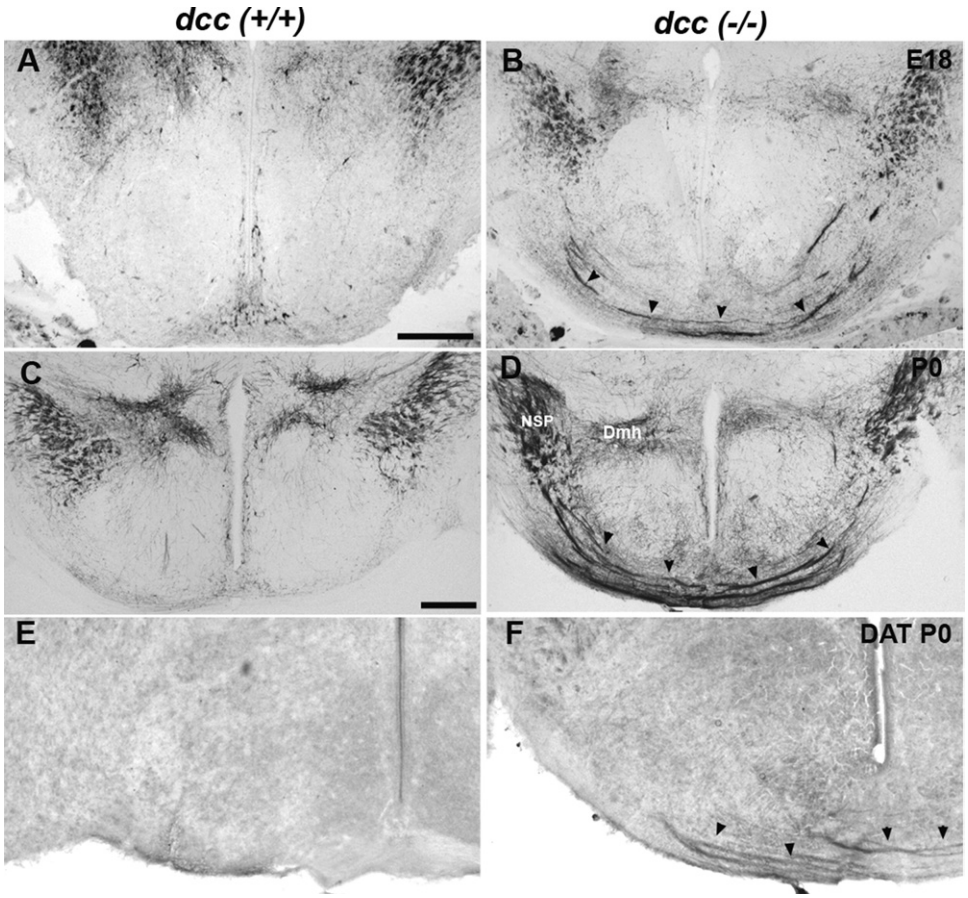

Fig. 6. Aberrant midline crossing of DA fibers in $dcc^{-/-}$ mice. (A–D) Representative TH-immunostained sections of $dcc^{+/+}$ (A, C) or $dcc^{-/-}$ (B, D) mice. In $dcc^{+/+}$ mice, TH-positive fibers originate from the SN and project to the ipsilateral striatum, forming the nigrostriatal pathway (NSP) (A, C). Loss of DCC function results in bundles of TH-positive fibers forming an abnormal projection across the midline at the level of the hypothalamus (black arrowheads B, D). Dopamine transporter immunoreactivty confirms the DA identity of abnormal commissural fibers detected in $dcc^{-/-}$ mice (F), that are absent in wild type littermates (E). Dmh, dorsal medial hypothalamic nucleus. (E, F) Representative slides stained for dopamine transporter (DAT). Scale bar=300 μm.

Layer II/III of prefrontal cortex in adult $dcc^{+/-}$ heterozygotes compared to wild-type littermates (Fig. 8B–E, G). No significant difference in TH-immunoreactive fiber density was detected in Layer V/VI.

To determine if the density of DA puncta, characteristic of axonal varicosities, was altered in adult DCC deficient mice, we counted TH-immunoreactive puncta in optical sections of the superficial layers of cingulate cortex imaged using confocal microscopy. Consistent with the increase in surface area occupied by TH-immunoreactive axons in medial prefrontal cortex of adult $dcc^{+/-}$ hetereozygotes, a ~30% increase of TH-positive puncta in the superficial layers of medial prefrontal cortex was observed in adult $dcc^{+/-}$ hetereozygous mice compared to wild-type littermates (Fig. 8I–L).

Homozygous $dcc^{-/-}$ null mice die shortly after birth (Fazeli et al., 1997). Newborn P0 pups were therefore used to investigate the innervation of DA fibers within the prefrontal cortex of $dcc^{-/-}$ null mice (Fig. 9). The thickness of the prefrontal cortex did not differ between genotypes (Fig. 9E). Although decreased DCC expression in $dcc^{+/-}$ heterozygotes generates an increase in the density of DA fibers detected in adulthood, $dcc^{-/-}$ null mice exhibited a significant decrease of TH-immunoreactive fibers in prefrontal cortex compared to wild-type littermates at P0 (Fig. 9D). This severe disruption of innervation in knockouts indicates that DCC is essential for the majority of DA axons to appropriately target the medial prefrontal cortex. Interestingly, in $dcc^{+/-}$ heterozygous pups at P0, the medial prefrontal cortex exhibits a trend toward increased innervation by TH positive axons, although this does not reach the threshold of statistical significance. This finding suggests that the significantly increased DA axon elaboration detected in the prefrontal cortex of adult $dcc^{+/-}$ heterozygotes (Fig. 8G) results from axonal arborization that occurs postnatally.

Netrin-1 increases axon length and axon branching of embryonic MDNs *in vitro*

Netrin-1 promotes DA axon extension from explants of E14 rat ventral midbrain grown in collagen gel cultures (Lin et al., 2005). In addition to promoting axon out-

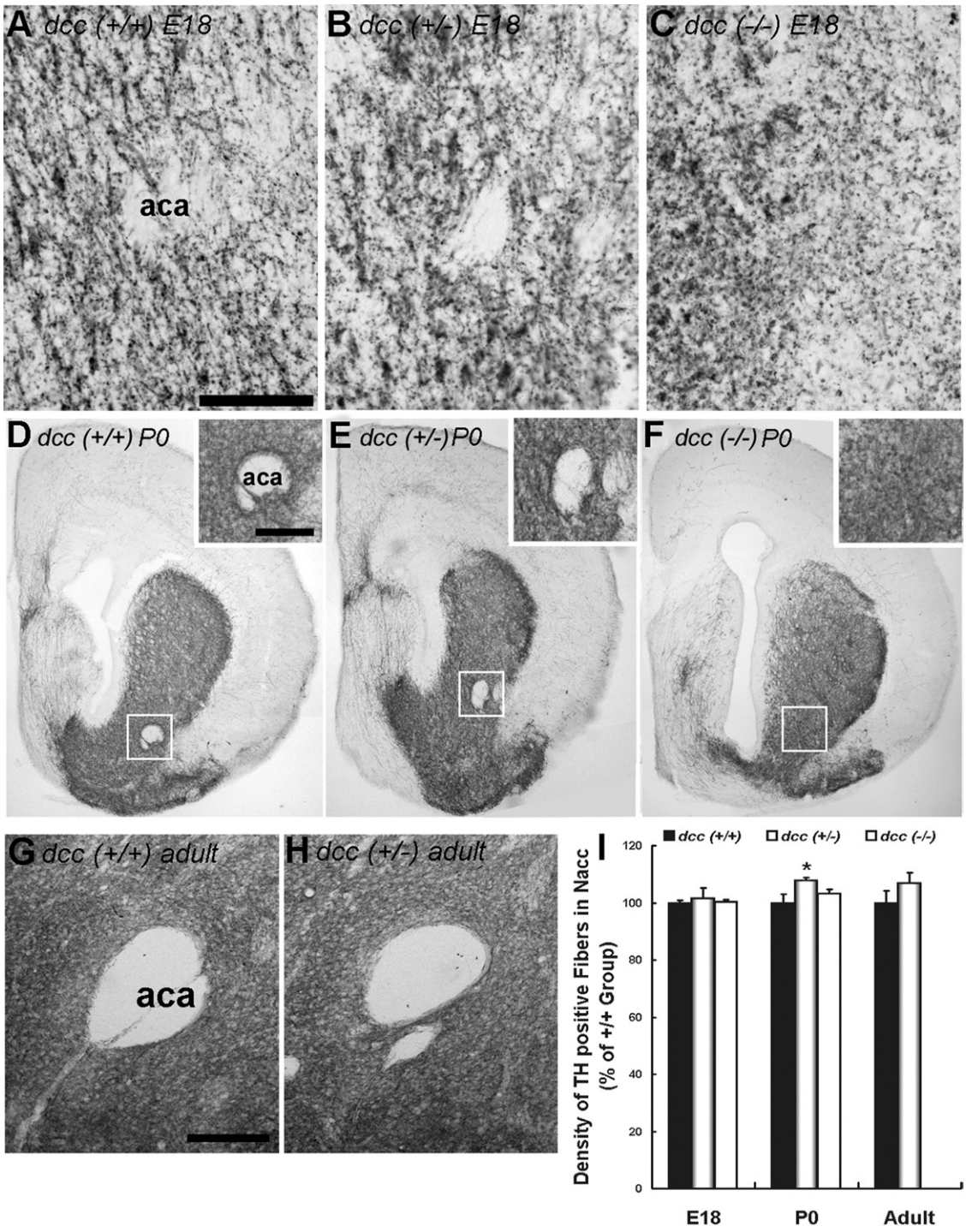

Fig. 7. TH-positive innervation of nucleus accumbens core (AcbC) at P0. (A–H) Representative sections of TH-labeling within AcbC at comparable rostal–caudal levels of $dcc^{+/+}$ wild-type (A, D, G), $dcc^{-/-}$ null (C, F), and $dcc^{+/-}$ heterozygous (B, E, H) mice. The anterior commissure is absent in $dcc^{-/-}$ mice (Fazeli et al., 1997). The white boxes (D, E, F) outline the regions magnified in the inserts presented in the upper right corner of each panel. No difference in density of TH innervation of the AcbC is found between $dcc^{-/-}$ and $dcc^{+/+}$ at E18 or P0. A small significant increase of TH-immunoreactivity (TH-IR) was detected in $dcc^{+/-}$ compared to wild-type ($dcc^{+/+}$) littermates at P0. Scale bar=200 μm. aca, anterior commissure, anterior limb. (I) Histogram illustrating TH-immunoreactivity as measured by the average grey value within AcbC. The * indicates a significant increase of TH-IR detected in $dcc^{+/-}$ heterozygotes compared with wild-type mice at P0 (ANOVA and post-hoc Tukey test, $P<0.05$; E18: $n=5$, 4, and 4 for wild-type, heterozygotes, and knockout mice; P0: $n=4$, 4, and 6; adult $n=5$ for wild-type and heterozygotes).

growth, netrin-1 promotes axon branching by embryonic cortical neurons *in vitro* (Dent et al., 2004). Our findings provide evidence that netrin-1 may influence DA axonal arborization *in vivo*; however the changes detected

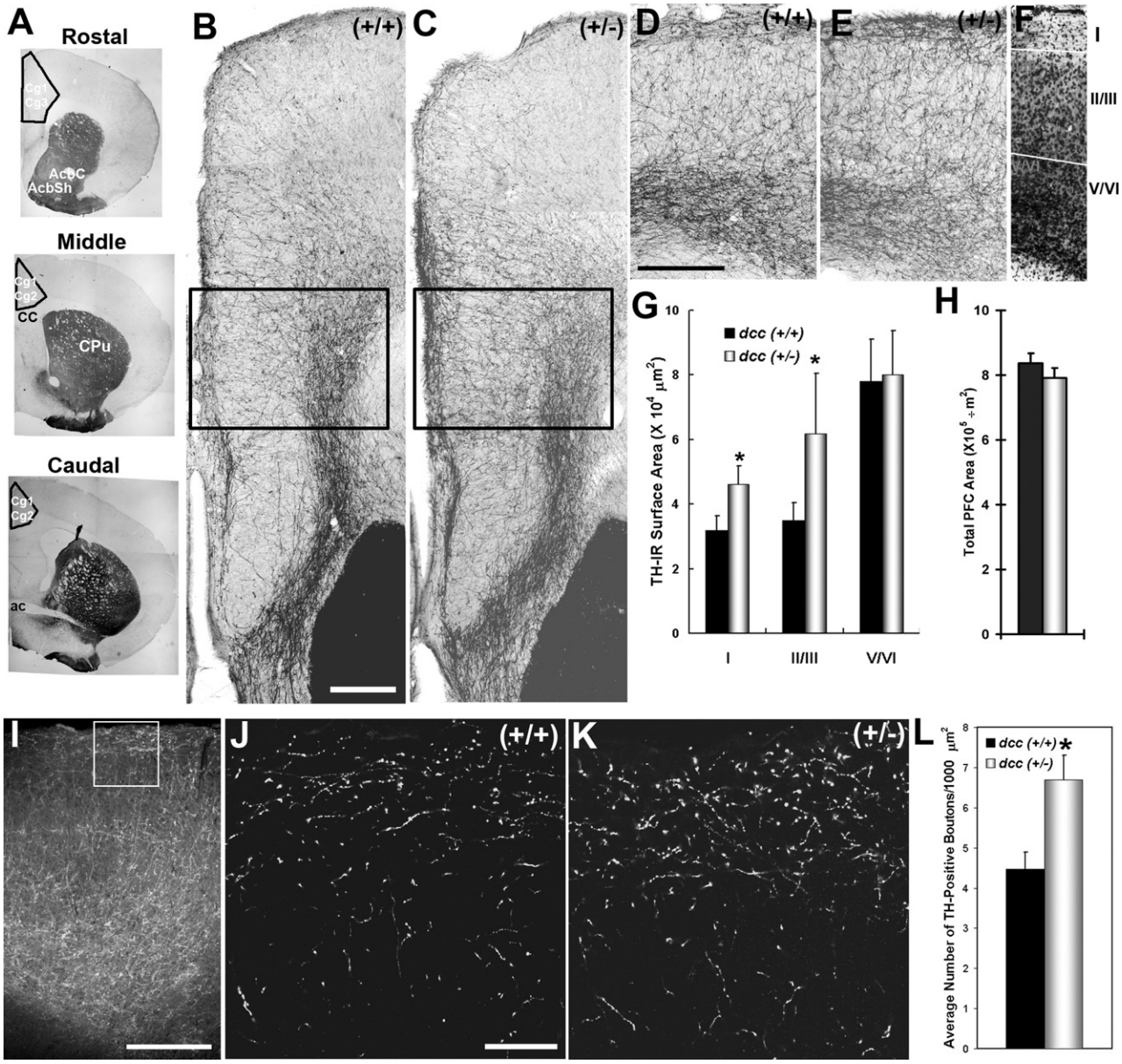

Fig. 8. Increased TH immunoreactivity in the prefrontal cortex of adult *dcc*$^{+/-}$ mice. (A) Illustration of sections double-stained with TH and Cresyl Violet showing the three rostal–caudal levels of prefrontal cortex examined. Cingulate cortex, area 1 (Cg1), 2 (Cg2) and 3 (Cg3) were included in the measurements. The rostral level was defined as the most rostral section in which the caudate putamen (CPu) was clearly visualized (A, top panel). The middle level was defined as the most rostal section in which the genu of corpus callosum (Gcc) first appears (A, middle panel). The caudal level is the most rostral section where the anterior commissure (aca) crossed the midline (A, bottom panel). The black frame within each section indicates the area being included in the measurement. AcbS, nucleus accumbens, shell; AcbC, nucleus accumbens, core; ac, anterior commissure; cc, corpus callosum. (B–E) Representative digital images of the prefrontal cortex taken from wild type *dcc*$^{+/+}$ (B, D) and *dcc*$^{+/-}$ heterozygous (C, E) mice. Panels (D, E) are images taken at higher magnification from the frame highlighted in panel (A, B). (F) Representative digital image of prefrontal cortex double stained with TH immunohistochemistry and Cresyl Violet showing the definition of layer I, layers II/III, and layers V/VI. The surface area occupied by TH-immunoreactivity was measured separately for each defined layer(s). (G) Adult *dcc*$^{+/-}$ mice had significantly more TH-positive fibers in layer I and layer II/III of the prefrontal cortex than *dcc*$^{+/+}$ mice (n=5 wild type and 5 heterozygotes; * ANOVA, $P<0.005$). (H) The measured area of the prefrontal cortex did not differ between genotypes (right panel). (I) Epifluoresent image of TH-immunoreactivity in the cingulate cortex taken from the rostral level described in panel (A). A 230×230 μm^2 frame (white) was placed on the superficial layers, including layer I and part of layer II. Digital confocal images were obtained, and TH-positive puncta within the frame were manually counted. (J, K) Confocal sections illustrating TH-positive puncta in the superficial layers of medial prefrontal cortex in *dcc*$^{+/+}$ and *dcc*$^{-/-}$ mice. (L) The average density of TH-positive puncta is significantly higher in adult *dcc*$^{+/-}$ heterozygotes compared to wild type *dcc*$^{+/+}$ littermates (n=6 wild type and 8 heterozygote litermate controls; two-way ANOVA, * $P<0.05$). Scale bars in (B, D), and (I) correspond to 300 μm, and in (J) to 50 μm.

could be due to loss of DA function in the innervating axons or within the target tissue itself. To test the hypothesis that netrin-1 regulates DA axonal branching, cultures containing DA neurons were prepared from dis-

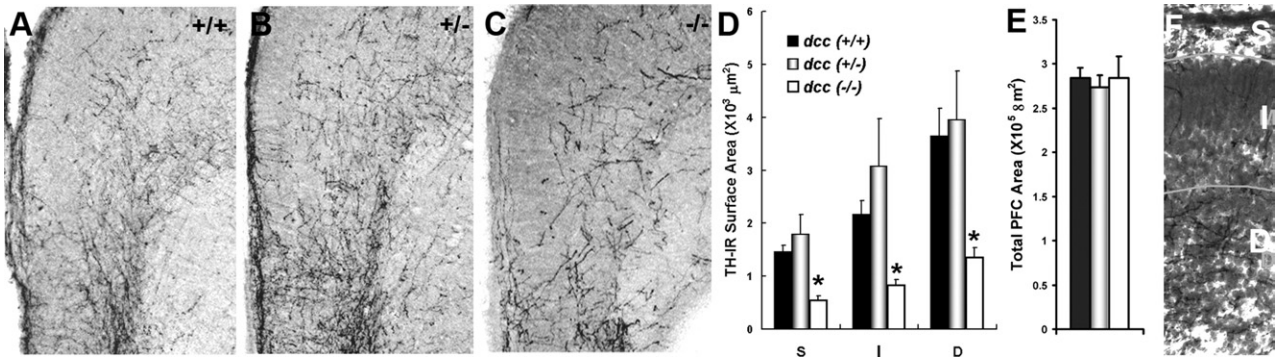

Fig. 9. TH immunoreactivity in the prefrontal cortex of P0 mice. (A–C) Representative TH-immunostained images taken from the prefrontal cortex of wild-type (+/+, A), heterozygous (+/−, B), and DCC mutant (−/−, C) newborn mice. (D) $Dcc^{-/-}$ mice have significantly fewer TH-positive fibers in all layers of the prefrontal cortex when compared with $dcc^{+/+}$ and $dcc^{+/-}$ mice. The measured area of the prefrontal cortex did not differ between the three genotypes (E). (F) Representative digital images of prefrontal cortex double-stained with TH (brown) and Cresyl Violet (blue) illustrating the definition of superficial (S), intermediate (I) and deep (D) layers at P0. (* ANOVA, post hoc Tukey test, $P<0.05$ compared to $dcc^{+/+}$ or $dcc^{+/-}$ genotype, $n=3$ P0 pups of each genotype).

sociated E13.5 mouse ventral mesencephalon. Following 8 DIV, DCC, netrin-1, UNC5A, and UNC5C were detected associated with the soma and neurites of TH-positive neurons (Fig. 10). Following 7 DIV, mesencephalic neurons were stimulated with either 200 ng/mL netrin-1, 10 μg/mL DCC function blocking monoclonal antibody (Keino-Masu et al., 1996), or netrin-1 plus DCC functional blocking antibody for 24 h. Cultures were then

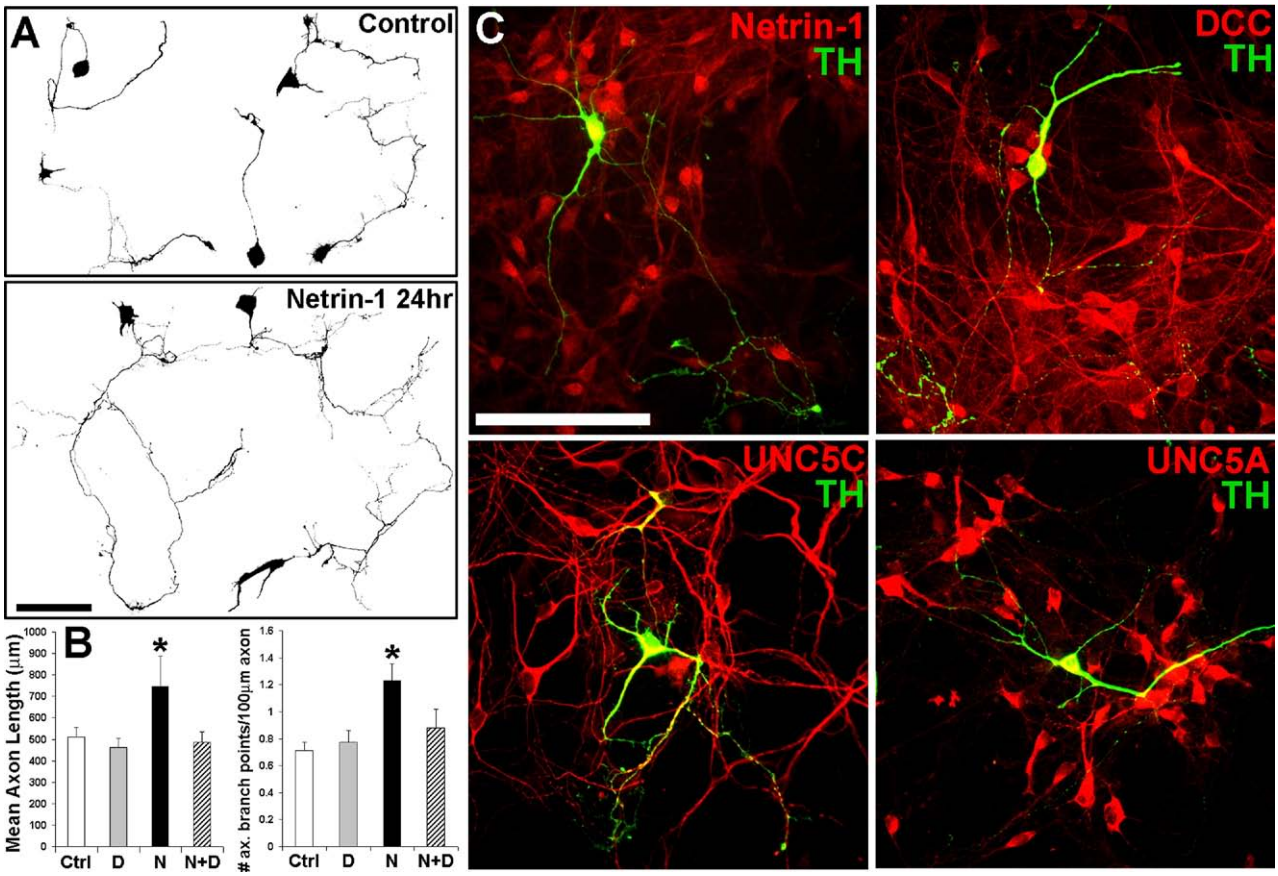

Fig. 10. Netrin-1 increases axon length and branching of mesencephalic TH-positive neurons in culture. (A) Images illustrating inverted immunofluorescence of ventral mesencephalic neurons cultured for 8 DIV labeled with TH. After 7 DIV, netrin-1 (200 ng/mL), netrin-1 and DCC function-blocking antibody (10 μg/mL), or vehicle alone, were bath applied to the cultures for 24 h. Scale bar: 50 μm. (B) Addition of netrin-1 for 24 h significantly increased axon length and branching. DCC function blocking antibody blocked both of these effects (* ANOVA, post hoc Tukey test, $P<0.01$ for both axon length and branching). (C) Netrin-1 and its receptors, DCC, UNC5A, and UNC5C are expressed by mesencephalic TH-positive neurons at 8DIV. Cells are stained with antibodies against netrin-1, DCC, UNC5A, or UNC5C (red), together with an antibody against TH (green). Scale bar: 100 μm.

fixed (8 DIV) with 4% PFA and DA neurons identified using TH immunohistochemistry. An axon was defined as the longest TH-positive neurite emerging from the cell body. The addition of exogenous netrin-1 for 24 h significantly increased both axon length and axon branching of TH positive cells compared to control conditions (Fig. 10B). We then assessed DCC function using a function blocking monoclonal antibody that has been demonstrated to block netrin-1 induced axon extension, cell migration, *dcc* and DCC signal transduction (Keino-Masu et al., 1996; Jarjour et al., 2003; Shekarabi et al., 2005). While application of DCC function blocking antibody alone for 24 h did not significantly affect baseline levels of axon length and branching, it abolished the increased axon branching induced by addition of netrin-1 (Fig. 10). These findings provide evidence that netrin-1 regulates DA axon extension and branching via a mechanism that is dependent on DCC.

Disruption of DCC function reduces the number of autaptic axon terminals formed by single postnatal DA neurons *in vitro*

To further reduce the complexity of the *in vitro* conditions and assess the contribution of DCC expressed by DA neurons to axonal arborization and synapse formation, DA neuronal microculture assays were used. In this model, neurons are cultured on micro-islands formed from droplets of substrate that limit synaptic connectivity to the cells within the micro-island. A single DA neuron grown on a micro-island of substrate establishes synaptic connections onto itself, called autapses, allowing the number of presynaptic specializations derived from a single isolated neuron to be quantified (Fasano et al., 2008). For this analysis, cells were dissociated from a block of tissue containing DA cell bodies microdissected from the level of the midbrain flexure from a newborn rat brain. Cells were then plated on collagen micro-islands and grown in astrocyte conditioned medium. DA neurons were identified based on TH immunoreactivity and presynaptic varicosities identified with an antibody against the synaptic vesicle protein SV2 (Fig. 11A, B). Mature DA neurons express readily detectable levels of netrin-1 *in vivo* (Livesey and Hunt, 1997) and *in vitro* (Fig. 10C). Treating the cells with exogenous netrin-1 (150 ng/mL), beginning at 2 DIV, again when changing the media at 4 DIV, and continuing to 7 DIV, did not alter the number of SV2 positive axon terminals formed by a cell (Fig. 11E), suggesting that in these conditions, DA neurons produce sufficient quantities of netrin-1 to saturate autapse formation. In contrast, chronic treatment with DCC function blocking antibody (10 μg/mL) at 2 and 4 DIV and assayed following 7 DIV, generated approximately 20% fewer autaptic SV2 positive varicosities per cell when compared to control conditions (Fig. 11C, D, F). We conclude that disrupting DCC function in DA neurons in these conditions reduces axonal arborization and the number of presynaptic terminal specializations formed per cell.

DISCUSSION

We report that loss of DCC function *in vivo* disrupts the migration of DA neuronal precursors, long-range guidance of DA axons to their targets, and DA axonal innervation within target zones. In the absence of DCC, an aberrant DA commissure forms in the ventral hypothalamus, and the distribution of DA innervation of the ventral striatum, including olfactory tubercle and nucleus accumbens shell, is malformed. In adult $dcc^{+/-}$ heterozygous mice, despite reduced numbers of DA neurons in the mesencephalon, innervation of the AcbC and medial prefrontal cortex by DA axons is either approximately equal to wild type, or enhanced, respectively. Furthermore, disrupting DCC function *in vitro* reduces axon extension, axon branching, and the elaboration of synaptic connections by DA neurons. These findings support the conclusion that DCC regulates DA neuronal precursor cell migration, axon guidance, and axonal terminal arborization.

DCC regulates DA precursor migration

We have previously reported significantly reduced numbers of midbrain DA neuronal cell bodies within the SNc and VTA of adult $dcc^{+/-}$ heterozygous mice (Flores et al., 2005). Here we report that at birth, the SNc and VTA of $dcc^{-/-}$ null mice contain further reduced numbers of DA cells. In contrast, in newborn $dcc^{+/-}$ heterozygous mice only the SNc contains fewer TH immunoreactive cells. We provide evidence that the decrease in TH immunoreactive cells within DA nuclei can be at least partly attributed to a migration deficiency, rendering many DA precursors unable to properly locate ventral mesencephalic nuclei between embryonic day 14 (E14) and birth. The floor plate of the mesencephalon and MDN precursors themselves express netrin-1 during the generation and migration of MDNs (Livesey and Hunt, 1997). We hypothesize that netrin-1 secreted by the floor-plate at the ventral midline may guide DA precursors ventral–rostrally as they migrate from the isthmic organizer. Alternatively, netrin-1 expressed by DA neurons may serve an autocrine function, influencing the rate or efficiency of migration. Wild type DA precursors express DCC at E14 (Fig. 2), during their ventrorostral-radial migration, and many DA cells are displaced dorsal to the VTA and SNC in $dcc^{+/-}$ and $dcc^{-/-}$ mice. While the absence of DCC expression by DA neurons likely contributes to generating this phenotype, we have not ruled out the possibility that loss of DCC function may also influence cell migration by altering the territory through which these cells migrate.

Although DA neurons were readily detected inappropriately located dorsal to mesencephalic DA nuclei in *dcc* null mice, our stereological cell count indicates that the number of displaced cells does not fully account for the total number of cells missing from these nuclei. We detected activated caspase-3 in a subset of these cells, indicative of apoptotic cell death (Riedl and Salvesen, 2007). Activation of apoptosis due to errors in cell migration or due to the failure of an axon to innervate its appropriate target, followed by the rapid clearance of the dying

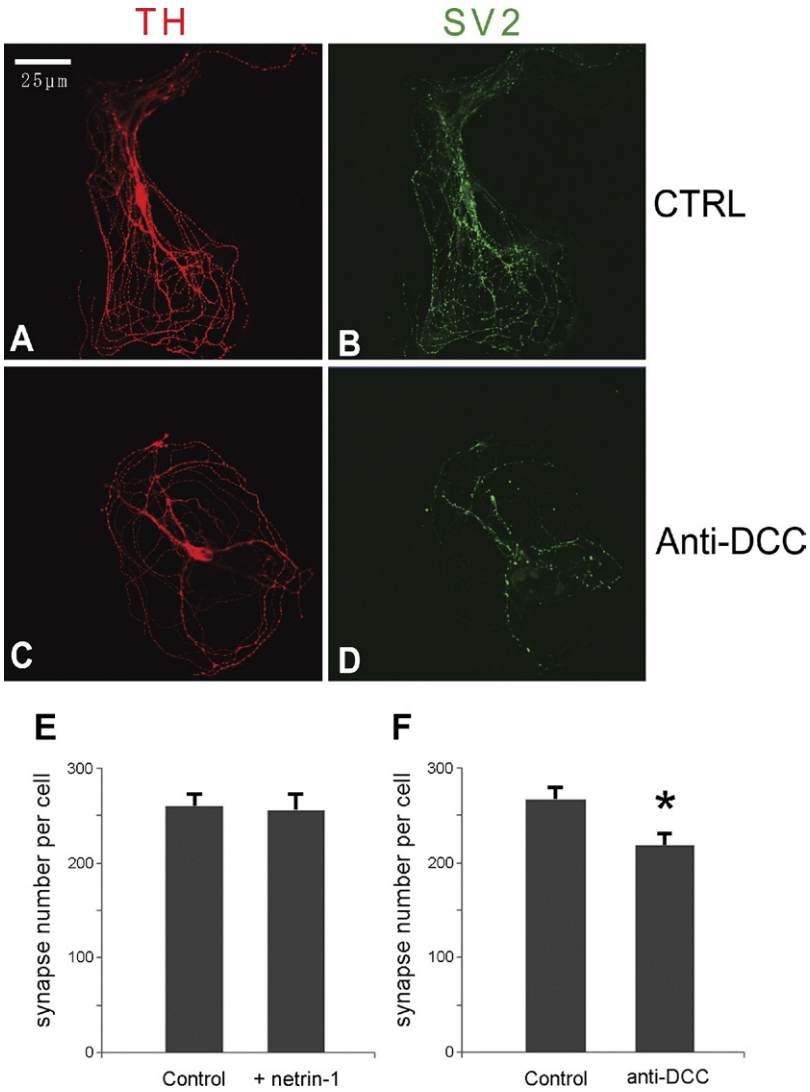

Fig. 11. Disrupting DCC function decreases the number of axon terminals established by single DA neurons in micro-island culture. (A–D) Single post-natal DA neurons restricted to micro-islands of substrate and co-immunostained for TH (red in A and C) and the synaptic vesicle marker SV2 (green in B and D). The DA neuron illustrated in panels (A) and (B) was cultured in control conditions, while the cell shown in panels (C) and (D) was cultured with the addition of DCC function-blocking monoclonal antibody. The number of presumed axon terminals was quantified by counting the number of varicosities positive for SV2. (E) Quantification of the number of autaptic presynaptic terminals established by individual cells in control conditions compared to cells cultured with the addition of recombinant netrin-1 protein from 2 DIV to 7 DIV (150 ng/mL; mean number of synapses per cell±SEM: control 262.1±16.8, n=41 cells; + netrin-1 259.5±20.3, n=45 cells; 2 tailed t-test P=0.923). (F) Quantification of the number of autaptic presynaptic terminals established by individual cells cultured in control conditions compared to those cultured with the addition of DCC function-blocking monoclonal antibody from 2 DIV to 7 DIV (10 μg/mL; mean number of synapses per cell±SEM: control 267.5±15.9, n=59 cells; DCC antibody 218.6±16.7, n=35 cells; 2 tailed t-test $P<0.05$ indicated by *).

cells, likely contributes to cells ultimately missing from mesencephalic DA nuclei. Additional studies will be required to determine if DCC may also influence DA cell proliferation or differentiation to account for the total reduction in the number of MDNs detected in DCC deficient mice.

Long-range DA axon guidance and short-range DA axon arborization

Axons of MDNs situated in the SNc and VTA exit ventral mesencephalic nuclei and travel rostrally within the MFB, comprising three major forebrain-directed pathways implicated in movement, motivation, and mood. Abnormalities in the development of each of these three major projections were detected in DCC deficient mice and are described below (summarized in Table 1).

Nigrostriatal pathway

Degeneration of the nigrostriatal pathway, a component of the ventral midbrain DA system, is a cause of the symptoms of Parkinson's disease. Notably, analysis of human single nucleotide polymorphisms detected in genes encoding proteins involved in axon guidance found that mutations in *dcc* were highly predictive of the age of onset and

Table 1. A qualitative summary of the changes in TH density and DA cell number found in brain regions of newborn (P0) *dcc* heterozygotes and *dcc* nulls, and in adult *dcc* heterozygotes, compared to age-matched wild type littermates. Arrows indicate an increase or decrease, while "=" indicates no change detected. The entries for VTA and SNc refer to the number of TH positive cells in these nuclei, while the entries for NAcc, PFC, and CPu refer to the density of TH innervation of these target structures. The table summarizes the findings presented here, and in our previous report (Flores et al., 2005)

	P0 DCC −/−	P0 DCC +/−	Adult DCC +/−
VTA	↓	=	↓
SNc	↓	↓	↓
NAcc	=	↑	=
PFC	↓	=	↑
CPu	=	=	=

susceptibility to develop Parkinson's disease (Lesnick et al., 2008; Lin et al., 2009), suggesting that DCC may contribute to maintaining nigrostriatal function.

In our current study, we detected an aberrant DA ventral commissure descending from the MFB and crossing the midline at the level of the hypothalamus in $dcc^{-/-}$ null mice, but never in $dcc^{+/-}$ heterozygotes or wild type littermates. Interestingly, a similar aberrant DA commissure descending from the MFB has been observed in mice lacking either the homeobox gene Nkx2.1 (Kawano et al., 2003), or the axon guidance cues, Slit1 and Slit2 (Bagri et al., 2002). Slit1, Slit2, and netrin-1 are highly expressed at the ventral midline (Kennedy et al., 1994, 2006; Bagri et al., 2002), and both slits and netrins contribute to preventing axons from inappropriately crossing the midline. The presence of the aberrant ventral commissure detected in all three loss-of function phenotypes may result from the failure of a subset of DA axons to respond to a cue that would normally repel them from the ventral midline and thereby restrict axons to ipsilateral trajectories. In Pax6 mutants, which exhibit an abnormal ventral to dorsal expansion of netrin-1 expression, TH-immunoreactive fibers from SN and VTA are deflected dorsally away from the ventral midline in the diencephalon (Vitalis et al., 2000), consistent with netrin-1 functioning in the ventral diencephalon as a repellent that inhibits axon growth. Netrin-1 evokes DA axon outgrowth from explants of E14 rat ventral midbrain *in vitro* (Lin et al., 2005), however this does not exclude the possibility that netrin-1 may function as a repellent for the same axons later along their trajectory. In fact, retinal ganglion cell axons initially respond to netrin-1 as a chemoattractant as they exit the eye but are subsequently repelled by netrin-1 as they approach their final target (Shewan et al., 2002). This study indicated that a single axon can switch between attraction and repulsion at different points along its trajectory. It remains to be determined if all DA axons respond uniformly to netrin-1 or if subsets of DA axons respond differently. Considering the diversity of the projections and functions of the various subpopulations of MDNs, it would be unlikely that all DA axons respond to the same guidance cue in the same way. Furthermore, although the aberrant ventral commissures formed in the Slit and netrin-1 knockout mice appear similar, it remains to be determined if these are composed of the same or different subpopulations of DA axons. An intriguing possibility is that these may be two distinct subpopulations of DA axons that respond to different midline repellent cues, but generate a superficially similar phenotype when the cue is absent.

Although abundant DCC protein has been detected in DA terminal fields of the neostriatum in the adult rat (Osborne et al., 2005), in spite of reduced DA cell numbers, no significant change in the morphology or density of TH innervations of the neostriatum was detected in $dcc^{+/-}$ heterozygous or $dcc^{-/-}$ null mice at birth, indicating that loss of DCC results in enhanced arborization of the remaining MDNs that innervate the dorsal striatum. This finding is consistent with our previous report that found no significant difference between levels of TH, DA or the DA metabolites DOPAC and HVA in the neostriatum of adult wild type and $dcc^{+/-}$ heterozgote aged matched littermates (Flores et al., 2005). We do not rule out the possibility that the application of higher resolution techniques may reveal more subtle alterations in the distribution of DA innervation in the neostriatum that result from changes in DCC expression.

Mesostriatal pathway

The mesostriatal pathway is comprised of axons originating in the VTA and terminating within the ventral striatum. In $dcc^{-/-}$ null mice, this projection shifts dorsally. It remains to be determined if this results from the mistargeting of DA afferents, or if the loss of DCC function produces a malformation of the targets of these axons, the Acbs and olfactory tubercle. No such aberration was observed in $dcc^{+/-}$ heterozygotes or wild type mice. Other areas of the ventral striatum, including ventral pallidum, and nucleus accumbens core, appear normal in both $dcc^{+/-}$ heterozygotes and null mice. TH immunoreactivity found in AcbC of $dcc^{-/-}$ null mice was not significantly different from that detected in wild type littermates at P0. However, a small but significant increase of TH-immunoreactivity was found in $dcc^{+/-}$ heterozygous littermates at birth. The significance of these findings must be considered in light of the 20 to 40% decrease in the number of mesencephalic DA neurons detected in $dcc^{+/-}$ heterozygotes and $dcc^{-/-}$ null mice at P0 (Fig. 2) and in adults (Flores et al., 2005). That the levels of TH positive staining in the terminal fields of mesencephalic DA axons was essentially normal in spite of reduced cell numbers suggests increased local axon arborization in the striata of $dcc^{+/-}$ heterozygotes and nulls. These findings are consistent with DCC influencing the extent of DA axon arborization innervating the striatum, with reduced levels of DCC correlated with increased arborization. Netrin-1 regulates embryonic cortical neuron axon branching (Kennedy, 2000; Dent et al., 2004), in addition to its role as a long-range guidance cue. Our findings provide evidence that DCC expressed by DA neurons inhibits local axon arborization in the ventral striatum.

Mesocortical pathway

The density of TH immunoreactive fibers in the prefrontal cortex of newborn $dcc^{-/-}$ null mice was substantially reduced, likely as a result of both reduced numbers of DA neurons and deficits in DA axon guidance. In contrast, TH immunoreactivity in the medial prefrontal cortex of $dcc^{+/-}$ heterozygotes exhibited a trend toward increased density at P0, and a significant increase in the adult, particularly in superficial cortical layers. We hypothesize that DCC mediates the response to a short-range repulsive guidance cue, perhaps a netrin, thereby inhibiting axon arborization in the prefrontal cortex that occurs relatively late in development, and that reduced DCC function in $dcc^{+/-}$ heterozygous mice compromises inhibitory signaling by a DCC–UNC5 homologue complex, resulting in exuberant axon arborization. While this remains to be tested directly in these cells, it is consistent with previous demonstrations that disrupting DCC function compromises the capacity of migrating cells and axons to respond to netrin-1 as a chemorepellent (Hong et al., 1999; Jarjour et al., 2003; Moore et al., 2007).

In contrast to these *in vivo* findings, our studies *in vitro* indicate that DCC promotes DA axon arborization and synapse formation. This could be due to differences in the intrinsic maturation of DA neurons *in vivo* and *in vitro*, or result from the absence of neuomodulatory factors *in vitro* that regulate switching between chemoattraction and chemorepulsion *in vivo*. Netrins can serve as either chemoattractive or chemorepellent cues depending on the repertoire of netrin receptors expressed by the responding cell and the influence of neuromodulators that regulate the intracellular concentration of cyclic nucleotides such as cAMP (Hong et al., 1999; Moore et al., 2007). Furthermore, cells may switch their response during development or following contact with an intermediate target. Our findings suggest a developmental shift in the expression of DCC and UNC5 homologues in the MDN system during maturation. Robust DCC expression was detected early in embryonic development, while UNC5A was highly expressed in adults. We have previously noted a similar developmental shift of netrin receptor expression during the maturation of the rat spinal cord (Manitt et al., 2004) and suggested that this functions to inhibit inappropriate axon sprouting once appropriate connections have been established. Here, our findings provide evidence that appropriate levels of DCC expression in DA neurons projecting to medial prefrontal cortex restrains local axon arborization, which occurs late in development and continues after birth (Riddle and Pollock, 2003).

Our findings demonstrate that appropriate expression of the axon guidance receptor DCC is essential for the development of DA nuclei and circuitry. Complete loss of DCC function results in gross axon pathfinding deficits and disorganization of DA terminal fields within the ventral striatum and cortex. The more subtle disruption of local DA terminal arborization in the limbic striatum and cortex found in $dcc^{+/-}$ heterozygotes indicates that precise regulation of DCC expression is critical for appropriate development of DA circuitry.

Acknowledgments—We thank Katherine Horn for comments on the manuscript. This work was supported by the Canadian Institutes of Health Research (CIHR). BX was supported by a Savoy Foundation Fellowship. TEK is a Killam Foundation Scholar and holds a Chercheur Nationaux award from the Fonds de la Recherche en Santé du Québec.

REFERENCES

Aoyagi A, Nishikawa K, Saito H, Abe K (1994) Characterization of basic fibroblast growth factor-mediated acceleration of axonal branching in cultured rat hippocampal neurons. Brain Res 661: 117–126.

Bagri A, Marin O, Plump AS, Mak J, Pleasure SJ, Rubenstein JL, Tessier-Lavigne M (2002) Slit proteins prevent midline crossing and determine the dorsoventral position of major axonal pathways in the mammalian forebrain. Neuron 33:233–248.

Berger B, Di Porzio U, Daguet MC, Gay M, Vigny A, Glowinski J, Prochiantz A (1982) Long-term development of mesencephalic dopaminergic neurons of mouse embryos in dissociated primary cultures: morphological and histochemical characteristics. Neuroscience 7:193–205.

Dalhstrom A, Fuxe K (1964) Evidence for the existence of monoamine-containing neurons in the central nervous system. I. Demonstration of monoamines in the cell bodies of brain stem neurons. Acta Physiol Scand 62:1–55.

Dent EW, Barnes AM, Tang F, Kalil K (2004) Netrin-1 and semaphorin 3A promote or inhibit cortical axon branching, respectively, by reorganization of the cytoskeleton. J Neurosci 24:3002–3012.

Fasano C, Thibault D, Trudeau LE (2008) Culture of postnatal mesencephalic dopamine neurons on an astrocyte monolayer. Curr Protoc Neurosci Chapter 3: Unit 3.21.

Fazeli A, Dickinson SL, Hermiston ML, Tighe RV, Steen RG, Small CG, Stoeckli ET, Keino-Masu K, Masu M, Rayburn H, Simons J, Bronson RT, Gordon JI, Tessier-Lavigne M, Weinberg RA (1997) Phenotype of mice lacking functional deleted in colorectal cancer (Dcc) gene. Nature 386:796–804.

Flores C, Manitt C, Rodaros D, Thompson KM, Rajabi H, Luk KC, Tritsch NX, Sadikot AF, Stewart J, Kennedy TE (2005) Netrin receptor deficient mice exhibit functional reorganization of dopaminergic systems and do not sensitize to amphetamine. Mol Psychiatry 10:606–612.

Franklin KBJ, Paxinos G (2008) The mouse brain in stereotaxic coordinates, pp 10010–11710. New York, NY: Elsevier, Academic Press.

Hong K, Hinck L, Nishiyama M, Poo MM, Tessier-Lavigne M, Stein E (1999) A ligand-gated association between cytoplasmic domains of UNC5 and DCC family receptors converts netrin-induced growth cone attraction to repulsion. Cell 97:927–941.

Hynes M, Rosenthal A (1999) Specification of dopaminergic and serotonergic neurons in the vertebrate CNS. Curr Opin Neurobiol 9:26–36.

Jarjour AA, Manitt C, Moore SW, Thompson KM, Yuh SJ, Kennedy TE (2003) Netrin-1 is a chemorepellent for oligodendrocyte precursor cells in the embryonic spinal cord. J Neurosci 23:3735–3744.

Kawano H, Horie M, Honma S, Kawamura K, Takeuchi K, Kimura S (2003) Aberrant trajectory of ascending dopaminergic pathway in mice lacking Nkx2.1. Exp Neurol 182:103–112.

Keino-Masu K, Masu M, Hinck L, Leonardo ED, Chan SS, Culotti JG, Tessier-Lavigne M (1996) Deleted in colorectal cancer (DCC) encodes a netrin receptor. Cell 87:175–185.

Kennedy TE (2000) Cellular mechanisms of netrin function: long-range and short-range actions. Biochem Cell Biol 78:569–575.

Kennedy TE, Serafini T, de la Torre JR, Tessier-Lavigne M (1994) Netrins are diffusible chemotropic factors for commissural axons in the embryonic spinal cord. Cell 78:425–435.

Kennedy TE, Wang H, Marshall W, Tessier-Lavigne M (2006) Axon guidance by diffusible chemoattractants: a gradient of netrin protein in the developing spinal cord. J Neurosci 26:8866–8874.

Leonardo ED, Hinck L, Masu M, Keino-Masu K, Ackerman SL, Tessier-Lavigne M (1997) Vertebrate homologues of C. elegans UNC-5 are candidate netrin receptors. Nature 386:833–838.

Lesnick TG, Sorenson EJ, Ahlskog JE, Henley JR, Shehadeh L, Papapetropoulos S, Maraganore DM (2008) Beyond Parkinson disease: amyotrophic lateral sclerosis and the axon guidance pathway. PLoS One 3:e1449.

Lin L, Lesnick TG, Maraganore DM, Isacson O (2009) Axon guidance and synaptic maintenance: preclinical markers for neurodegenerative disease and therapeutics. Trends Neurosci 32:142–149.

Lin L, Rao Y, Isacson O (2005) Netrin-1 and slit-2 regulate and direct neurite growth of ventral midbrain dopaminergic neurons. Mol Cell Neurosci 28:547–555.

Livesey FJ, Hunt SP (1997) Netrin and netrin receptor expression in the embryonic mammalian nervous system suggests roles in retinal, striatal, nigral, and cerebellar development. Mol Cell Neurosci 8:417–429.

Manitt C, Colicos MA, Thompson KM, Rousselle E, Peterson AC, Kennedy TE (2001) Widespread expression of netrin-1 by neurons and oligodendrocytes in the adult mammalian spinal cord. J Neurosci 21:3911–3922.

Manitt C, Thompson KM, Kennedy TE (2004) Developmental shift in expression of netrin receptors in the rat spinal cord: predominance of UNC-5 homologues in adulthood. J Neurosci Res 77:690–700.

Marchand R, Poirier LJ (1983) Isthmic origin of neurons of the rat substantia nigra. Neuroscience 9:373–381.

Moore SW, Tessier-Lavigne M, Kennedy TE (2007) Netrins and their receptors. Adv Exp Med Biol 621:17–31.

Osborne PB, Halliday GM, Cooper HM, Keast JR (2005) Localization of immunoreactivity for deleted in colorectal cancer (DCC), the receptor for the guidance factor netrin-1, in ventral tier dopamine projection pathways in adult rodents. Neuroscience 131:671–681.

Riddle R, Pollock JD (2003) Making connections: the development of mesencephalic dopaminergic neurons. Brain Res Dev Brain Res 147:3–21.

Riedl SJ, Salvesen GS (2007) The apoptosome: signalling platform of cell death. Nat Rev Mol Cell Biol 8:405–413.

Serafini T, Colamarino SA, Leonardo ED, Wang H, Beddington R, Skarnes WC, Tessier-Lavigne M (1996) Netrin-1 is required for commissural axon guidance in the developing vertebrate nervous system. Cell 87:1001–1014.

Shatzmiller RA, Goldman JS, Simard-Emond L, Rymar V, Manitt C, Sadikot AF, Kennedy TE (2008) Graded expression of netrin-1 by specific neuronal subtypes in the adult mammalian striatum. Neuroscience 157:621–636.

Shekarabi M, Kennedy TE (2002) The netrin-1 receptor DCC promotes filopodia formation and cell spreading by activating Cdc42 and Rac1. Mol Cell Neurosci 19:1–17.

Shekarabi M, Moore SW, Tritsch NX, Morris SJ, Bouchard JF, Kennedy TE (2005) Deleted in colorectal cancer binding netrin-1 mediates cell substrate adhesion and recruits Cdc42, Rac1, Pak1, and N-WASP into an intracellular signaling complex that promotes growth cone expansion. J Neurosci 25:3132–3141.

Shewan D, Dwivedy A, Anderson R, Holt CE (2002) Age-related changes underlie switch in netrin-1 responsiveness as growth cones advance along visual pathway. Nat Neurosci 5:955–962.

Shimoda K, Sauve Y, Marini A, Schwartz JP, Commissiong JW (1992) A high percentage yield of tyrosine hydroxylase-positive cells from rat E14 mesencephalic cell culture. Brain Res 586:319–331.

Shults CW, Hashimoto R, Brady RM, Gage FH (1990) Dopaminergic cells align along radial glia in the developing mesencephalon of the rat. Neuroscience 38:427–436.

Tong J, Killeen M, Steven R, Binns KL, Culotti J, Pawson T (2001) Netrin stimulates tyrosine phosphorylation of the UNC-5 family of netrin receptors and induces Shp2 binding to the RCM cytodomain. J Biol Chem 276:40917–40925.

van den Munckhof P, Luk KC, Ste-Marie L, Montgomery J, Blanchet PJ, Sadikot AF, Drouin J (2003) Pitx3 is required for motor activity and for survival of a subset of midbrain dopaminergic neurons. Development 130:2535–2542.

Vitalis T, Cases O, Engelkamp D, Verney C, Price DJ (2000) Defect of tyrosine hydroxylase-immunoreactive neurons in the brains of mice lacking the transcription factor Pax6. J Neurosci 20:6501–6516.

Volenec A, Zetterstrom TS, Flanigan TP (1998) 6-OHDA denervation substantially decreases DCC mRNA levels in rat substantia nigra compacta. Neuroreport 9:3553–3556.

Voorn P, Kalsbeek A, Jorritsma-Byham B, Groenewegen HJ (1988) The pre- and postnatal development of the dopaminergic cell groups in the ventral mesencephalon and the dopaminergic innervation of the striatum of the rat. Neuroscience 25:857–887.

(Accepted 12 May 2010)
(Available online 21 May 2010)